TECHNICAL PAPER

Influence of Tool Shoulder Concave Angle and Pin Profile on Mechanical Properties and Microstructural Behaviour of Friction Stir Welded AA7075-T651 and AA6061 Dissimilar Joint

Yuvaraj Kunnathur Periyasamy[1] · **Ashoka Varthanan Perumal[1]** ·
Boopathiraja Kunnathur Periyasamy[2]

Abstract In this present study, an attempt has been made to investigate the influence of tool shoulder concave angle and pin profile on mechanical properties and microstructural behaviour of friction stir welded AA7075-T651 and AA6061 dissimilar joint. The concave profile tool shoulder with three different angles of 1.5°, 3° and 4.5° was employed. Besides, three different pin profiles like straight cylindrical, square and triangular were used to fabricate the FSW joints. The concave shoulder angle regulates the frictional heat, and the tool pin profile enhances the material flow to improve the mechanical properties of the joint. From this work, it was found that 3° concave shoulder profile with square pin exhibits the maximum tensile strength, hardness and bending angle of 298 N/mm^2, 143 Hv and 49°, respectively. The pulsating stirring action of the square tool pin exhibits ductile fracture, and it is evident from the presence of fine dimples.

Keywords Friction stir welding · Tool shoulder profile · Tool pin profile · Tensile strength · Microhardness · Bending strength

✉ Yuvaraj Kunnathur Periyasamy
cadyuva94@gmail.com

Ashoka Varthanan Perumal
ashokavarthanan@skcet.ac.in

Boopathiraja Kunnathur Periyasamy
boopathiraja3177@gmail.com

1 Sri Krishna College of Engineering and Technology, Coimbatore, India

2 Sri Krishna College of Technology, Coimbatore, India

1 Introduction

Nowadays, material selection and manufacturing method play a vital role in the aircraft, aerospace and automobile industries by considering the fuel economy and safety aspects of passengers. Engineers are working on the architecture of vehicles from small sized fasteners to huge sized components for reducing the weight of existing designs. The first choice of the designer is aluminium material, which dominates the lightweight production and saves weight up to 50%. Al–Mg–Si alloys (6000 series alloys) are used for the comfortable handle and robust construction, but Al–Zn–Mg alloys (7000 series alloys) are explicitly chosen for high strength applications. In this research work, dissimilar AA7075-T651 and AA6061 joint has been fabricated by employing friction stir welding process, and it will throw some light on the strength of dissimilar joint when compared to the parent material. Friction stir welding is a clean, simple, innovative and attractive solid-state welding process for fabricating aluminium and its alloys which have difficulties in hot cracking and grain boundary liquation in conventional fusion welding technique due to the loss of alloying elements in the fusion heat.

In the FSW process, an inconsumable tool with shoulder [1] arrangement generates the heat and material plastic deformation due to frictional contact between the top surface of the workpiece and the bottom of the shoulder. At the same time, tool pin which penetrates inside the butt joint of material can stir the plasticized material [2] to flow from retreading side to advancing side and vice versa. The FSW joint comprises of four different regions [3] such as (a) weld nugget zone (WNZ), (b) heat-affected zone (HAZ), (c) thermomechanically affected zone (TMAZ) and (d) parent material zone (PM). Selection of tool material

and geometry are closely related to the performance of the joint. The tool shoulder size and profile play a dynamic role in influencing the material flow and strength of the weld joint. Tool shoulder with a concave and convex profile can enhance the plastic flow of material and act as a reservoir.

The function of FSW tool pin shear is to shear the plastically deformed material and transfer it from retreating side to advancing side of the weld zone. The amount of material to be sheared from the plasticized region [4] can be varied with the tool pin profile (cylindrical, square, tapered, threaded and triangle). Galvao et al. [5] made an attempt to investigate the influence of three different tool shoulder profiles like flat, conical and scrolled on mechanical properties and microstructure behaviour of 1-mm-thick copper-DHP plates. Tool rotational speed and traverse speed can be varied for all the three shoulder profiles. There is no separation between shoulder-driven and pin-driven zones due to higher volume of material dragged by the shoulder with scrolled profile, which reveals good flow of material through thickness. From the experimental results, it is reported that the tool shoulder with scrolled profile exhibits fine grains with higher tensile strength and hardness. Similarly, Mugada et al. [6] used the tool shoulder with different end features to observe the temperature generation and mechanical properties of friction stir welded AA6082 joint. They found that almost 32% of the load reduces while using the tool shoulder with ridges when compared to the other tools. In the RST (ridges shoulder tool), the plasticized material passing through the re-entrant shears off continuously at multiple locations during both translational and rotational motions of the tool. Furthermore, the joint fabricated with RST satisfies the criteria of temperature generation and exhibits better mechanical properties.

In another attempt, Leal et al. [7] reported that the tool shoulder with conical cavity enhances the material flow with onion ring structure. The tool shoulder with scrolled profile induces more amount of plastic deformation when compared to conical profile, which is directly proportional to the nucleation of new grains in the weld stir zone. On the other hand, the joint fabricated with scrolled shoulder exhibits an extensive mixing of material throughout the thickness. The lowest possible heat generated by scrolled shoulder tool refines the grain, which reveals maximum hardness and tensile strength. In a similar attempt, Mugada et al. [9] analysed the material flow and mechanical properties of friction stir welded AA6082 joint. The FSW joints are fabricated by using a tool shoulder with ridges and five different pin profiles such as polygon, octagon, hexagon, square and tapered cylindrical. The tool shoulder with ridges combined with square pin reveals uniform mixing and distribution of marker material along the retreating and advancing side due to adequate shearing of

marker material with minimal sticking length. Therefore, the square tool pin exhibits the maximum tensile strength and hardness with the uniform distribution of material in the weld nugget zone (WNZ).

Scilapi et al. [9] investigated the effect of tool shoulder geometries on mechanical properties and microstructural behaviour of friction stir welded AA6082 joint. The tool shoulder with three different types of profiles like cavity and fillet, scroll and fillet and only fillet has been employed for fabricating the joint. The tool shoulder with fillet and cavity exhibits very little flashes and smooth surface due to the removal of flash as a continuous chip. The cavity prevents the escaping of plasticized material away from the weld stir zone (WSZ), and it forms a compressed ring of plasticized material around the tool pin. They confirmed that the tool shoulder with fillet and cavity is the best choice for welding the sheets with 1.5 mm thickness. Similarly, Trueba et al. [10] analysed the tensile properties and defects of friction stir welded AA6061-T6 alloy by using six different tool shoulder features. The six tools are fabricated by using metallic additive manufacturing technology. Tensile and non-destructive testing is used to evaluate the weld strength. The raised spiral profile eliminates the excessive flash formation by directing the deformed material towards the centre of stirring pin. Moreover, the wiper improves the surface finish of the weld by smoothing the metal after weld. The FSW tool with raised spiral shoulder produces the defect-free weld with the maximum tensile strength of 209.3 Mpa.

Few authors have attempted to investigate the influence of tool pin profile on the mechanical and microstructural behaviour of friction stir welded joint. Palanivel et al. [11] observed the macroscopic defects in the weld zone due to overaging of precipitates and variation in the material flow pattern. The dissimilar AA5083-H111 and AA6351-T6 joint is fabricated by employing five different tool pin profiles at three different tool rotational speeds of 600 rpm, 950 rpm and 1300 rpm. The mixed flow region of the weld is influenced by tool pin profile and rotational speed. The variation in tool pin profile and speed is attributed to dissolution and overaging of precipitates. Therefore, the FSW joint fabricated by using the straight square pin and the rotational speed of 950 rpm yields the maximum tensile strength of 273 MPa.

Similarly, Mehta et al [12] investigated the influence of tool pin profile on the mechanical behaviour of friction stir welded dissimilar aluminium and copper joints. They reported that while increasing the polygonal edges of the tool pin, the fragmental defects get reduced. Moreover, less amount of heat is generated by the tool pin with 10 mm diameter which reveals improper material flow and lack of surface fill. On the other hand, large amount of Cu particles scratched by high input heat of 6-mm-diameter tool pin are

unable to mix with Al matrix resulting in defective stir zone. It is found that the square pin exhibits the maximum tensile strength and hardness due to the presence of intermetallic compounds like CuAl, $CuAl_2$, Cu_3Al and Cu_9Al_4 in the stir zone (SZ). Beygi et al. [13] in a further FSW tool pin study pointed out that threaded conical tool exhibits maximum tensile strength and hardness when compared to other joints fabricated with the tool pin profiles like pyramidal and threaded cylindrical. Moreover, they reported that downward material flow plays a vital role to eliminate macrodefects. At the same time, the upward material flow merges with the shoulder influenced region and prevents the defects on advancing side of the weld. The downward material flow in the threaded conical pin is not that much to affect the weaker interface at the retreating side which is inevitable.

In a similar attempt, Elangovan et al. [14] used the five different pin profiles (square, triangular, straight cylindrical, tapered cylindrical and threaded cylindrical) at three different welding speeds to analyse the friction stir processing zone in the AA2219 joint. The eccentricity associated with the flat faced tool profiles like square and triangle pin allows the incompressible material to flow around the pin with pulsating stirring action. They found that square tool pin exhibits defect-free weld with the maximum joint efficiency and hardness of 61% and 105 Hv, respectively. On the other hand, Ilangovan et al. [15] attempted to investigate the influence of tool pin profile on the mechanical behaviour of friction stir welded AA6061(heat treatable) and AA5086 (non-heat treatable) dissimilar joint. He observed the blunt complex flow of materials and defect-free stir zone by using a threaded pin tool. The pin influenced region of threaded pin consists of alternatively stacked equal quantity of AA6061 and AA5086 to form onion rings. Furthermore, the formation of fine grains improves the hardness and tensile strength value to 83 Hv and 169 MPa, respectively.

In another attempt, Elangovan et al. [16] analysed the mechanical behaviour of friction stir welded AA6061 joint by varying the tool pin profile and tool rotational speed. The tool pin profile with flat face like square and triangle exhibits fine grains and homogeneous redistribution of secondary particles in the weld stir zone due to pulsating stirring action. The FSW joints fabricated with square tool pin profile at 1200 rpm exhibit maximum tensile properties because of fine grains and uniform distribution of strengthening precipitates. Motalleb-nejad et al. [17] reported that the screw threaded and tapered cylindrical pin has improved the mechanical properties and microstructural behaviour of AZ31B magnesium alloy joints. The tool pin without screw thread exhibits poor plastic deformation because of low axial force and insufficient material flow. The oxides are trapped inside the weld stir zone, which

leads to the formation of "kissing bond" defect. Moreover, it has been found that the threaded tool and rotational tool speed dominate the joint strength when compared to the cylindrical pin and tool traverse speed.

Similarly, Bahrami et al. [18] used the five different tool pin geometries to analyse the mechanical properties and microstructural behaviour of friction stir welded AA7075/ Sic nano-composite joint. They found that tapered cylindrical and four flute tools exhibit maximum hardness due to uniform distribution of Sic nano-particles in the stir zone. Moreover, the joint fabricated with four flute tool exhibits severe accumulation of Sic nano-particles. According to the Hall–Petch relationship, the joint fabricated with the triangular tool exhibits very fine grains in the stir zone which reveals the maximum tensile strength.

The concave profile tool shoulder acts as a reservoir for the material sheared by the tool pin. As the tool moves forward in the welding, the deformed material from the stir zone is pushed into the shoulder cavity and again it is directed towards the tool pin. The flat tool shoulder exhibits large axial force on the weld stir zone and provides no escape volume for the deformed material. Therefore, the deformed material tries to flow upward and squeeze out of the rotating tool, known as flash out. By providing the concave profile in tool shoulder, the weld flash can be reduced.

Kim et al. [19] analysed the influence of tool shoulder with a concave and convex profile on the mechanical behaviour of friction stir spot welded joint. The outer diameter of the concave shoulder has the highest surface speed, which comes in contact with the material very early. Therefore, the top of the sheet material becomes softened earlier and the tool exhibits a steady state of force and torque when compared to convex. They found that the concave profile tool shoulder dominates the mechanical behaviour and exhibits better results. Similar to this, Zhang et al. [20] analysed the influence of the tool shoulder concave angle (0°, 5° and 10°) on mechanical behaviour of AA5052 joint. The FSW tool with 10° shoulder concave angle exhibits secondary sliding frictional heat between the base material and shoulder-driven material. This leads to the weakening of thermal shoulder effect and deteriorates the mechanical behaviour of AA5052 joint. Moreover, it has been found that the tool shoulder with concave profile angle of 0°–5° exhibits better mechanical properties.

The tool shoulder profile and tool pin profile play a vital role in heat generation, material mixing, material flow and mechanical behaviour of the friction stir welded dissimilar aluminium alloy joint. Most of the researchers found that the square, triangle and straight cylindrical tool pin profiles dominate the mechanical behaviour of friction stir welded joint. To the best of author's knowledge, the investigation on tool shoulder concave angle variation along with

Table 1 Chemical composition of AA7075-T651 and AA6061

Material	Cu	Mg	Zn	Cr	Fe	Si	Ti	Al
AA7075-T651	1.2–2	2.1–2.9	5.1–6.1	0.18–0.28	0.5	0.4	0.2	Remaining
AA6061	0.15–0.4	0.8–1.2	0.25	0.04–0.35	0.7	0.4–0.8	0.15	Remaining

different tool pin profiles for AA7075-T651 and AA6061 dissimilar alloys is limited. Furthermore, these two combinations of dissimilar aluminium alloys dominate the fabrication of fuselage, wings and main landing gear (MLG) links of aircrafts.

In this present study, influence of varying the concave angle of tool shoulder along with three different tool pin profiles, including straight cylindrical (SCT), square (ST) and triangle (TT) on mechanical properties and microstructural behaviour of friction stir welded AA7075-T651 and AA6061 dissimilar alloy joint, was elucidated.

2 Experimental Procedure

2.1 Material Selection

In this present study, dissimilar aluminium alloys of AA7075-T651 and AA6061 in the plate form with 6 mm thickness were welded by employing friction stir welding (FSW) process. The chemical composition and mechanical properties of the parent materials are tabulated in Table 1 and 2. The rolled plates were cut into the required size of 200 × 150 × 6 mm with the help of band saw machine. The silicon carbide sand paper was used to remove the pollutants [21] and metal oxide layers during surface and edge preparation of parent materials. The plate AA7075-T651 was kept at the retreating side and the plate of AA6061 on the advancing side.

2.2 Experimental set-up

The dissimilar AA7075-T651 and AA6061 FSW joint was fabricated by using single pass butt welding procedure. Experiments were conducted with the help of friction stir welding machine (model name: FSW 3T-300-NC) manufactured by R.V machine tools, which comprised of maximum spindle speed of 3000 rpm and Z-axis thrust force of

about 30kN as shown in Fig. 1. The FSW tool made of high-speed steel (HSS) with 20 mm shoulder diameter was used to weld the dissimilar joint. The butt joint plates were positioned correctly and clamped by using a special fixture. The trial experiments were conducted to determine the possible range of process parameters. The FSW process parameters [22] such as tool rotational speed of 2000 rpm, tool traverse speed of 60 mm/min, tool tilt angle of 2° (two degree), tool offset of 0.9 mm, tool pin diameter of 6 mm and axial force of 2kN were kept as constant. Compared to AA6061 material, the melting point of AA7075-T651 material is high. Therefore, the FSW tool was offset about 0.9 mm distance towards the AA7075-T651 material side to generate adequate frictional heat and stirring. Moreover, the FSW tool shoulder with three different concave angles (1.5°, 3° and 4.5°) and tool pin with three different profiles (straight cylindrical, square and triangle) were used as tool

Table 2 Mechanical properties of AA7075-T651 and AA6061

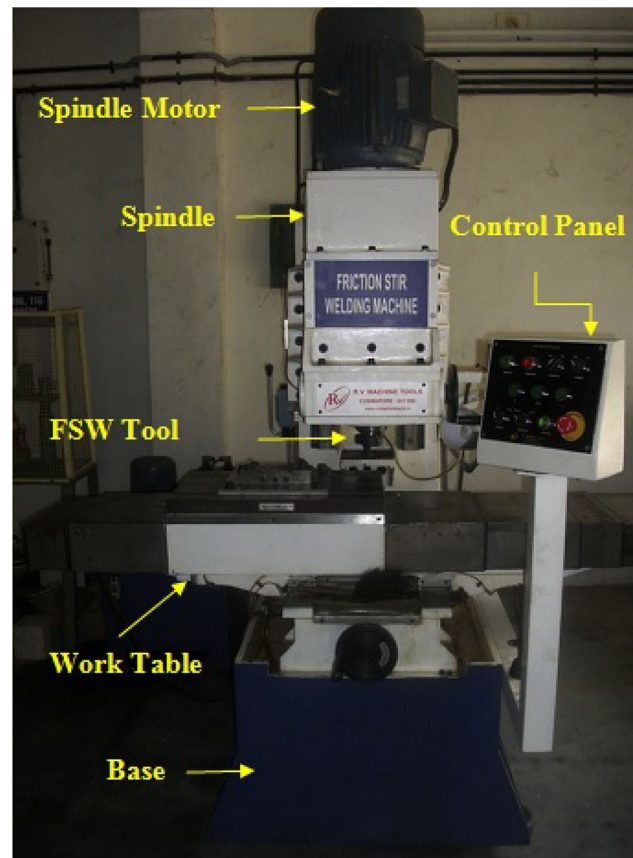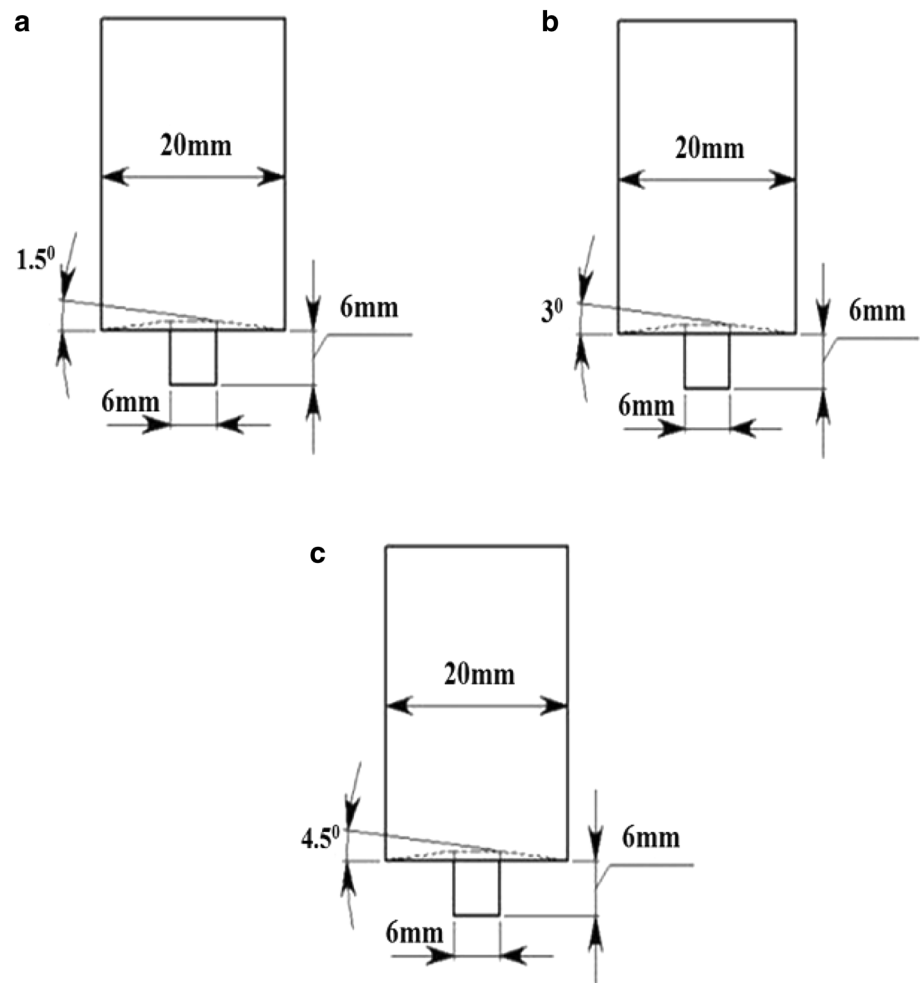| Material	Ultimate tensile strength/ Mpa	Yield strength/ Mpa	% Elongation
AA7075-T651	572	503	11
AA6061	310	276	12

Fig. 1 Friction stir welding machine set-up

Fig. 2 FSW concave profile tool shoulder with three different angles **a** 1.5°, **b** 3° and **c** 4.5°

geometry as shown in Figs. 2a–c and 3a–c, respectively. In this present study, nine different tool combinations (T1–T9) were employed to fabricate the dissimilar AA7075-T651 and AA6061 joints as shown in Fig. 4a–d.

### 2.3 Analysis of Mechanical Properties

2.3.1 Tensile Strength Measurement

The combinations of tool shoulder concave angle and tool pin profile have a prominent effect on tensile properties of the FSWed dissimilar joint. The tensile properties of the weld joint like yield strength, ultimate tensile strength and % elongation were measured under uniaxial tensile stress. The purpose of the tensile test was to compare the base material property and quality of the welded joint. As per the ASTM-E8M standards [23–28], transverse tensile specimens with the gauge length of 50 mm were extracted from the dissimilar welded plates smoothly with the help of EDM wire cutting as shown in Fig. 5. For each weld condition, three tensile specimens were prepared as shown

in Fig. 6. Average tensile values of these three specimens were considered for results and discussion. The computerized universal testing machine (UTM) with data acquisition system was used for the tensile test. The UTM crosshead was employed at a constant speed of 0.9 mm/min.

2.3.2 Microhardness Measurement

The microhardness value across the different zones of friction stir welded joint [29] could be measured with the help of Vickers microhardness tester. The transverse cross section of the welded sample was polished with different grades of emery sheets to remove the surface damage. Then, the microhardness was measured by applying 100 g of load for 15 s dwell time. Five to ten readings were taken at the different zones of the weld joint, and its average values were utilized for further discussion about microhardness.

Fig. 3 FSW tools with three different pin profiles **a** cylindrical, **b** square and **c** triangle
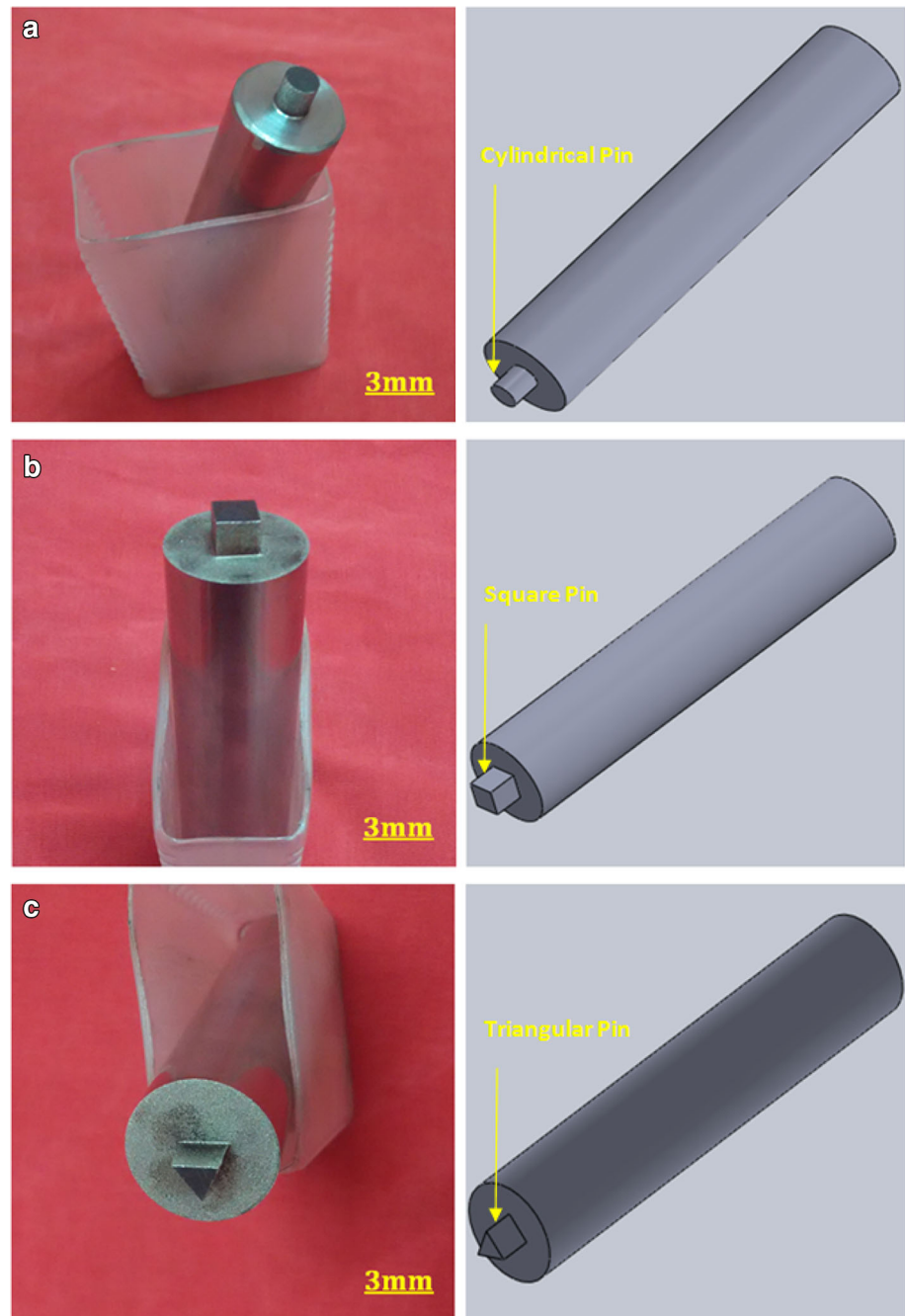
2.3.3 Bending Strength Measurement

The three-point bending test set-up along with roller arrangement which was available in the uniaxial fatigue testing machine was utilized for measuring the bending strength of the dissimilar weld joint. The crosshead speed of 1 mm/min was employed for conducting the bend test. Special fixture arrangement was available for both the fatigue test and three-point bending test.

2.4 Microstructure Characterization

The material flow, grain structure, grain size, presence of strengthening precipitates and the weld defects were revealed by the metallurgical characterization of transverse cross section extracted from the dissimilar AA7075-T651 and AA6061 welded joint. Weck's reagent etched the samples polished [30] with different grades of emery sheets. The digital camera and image analysing software incorporated with the optical microscope were utilized to record the microstructure across different regions of the
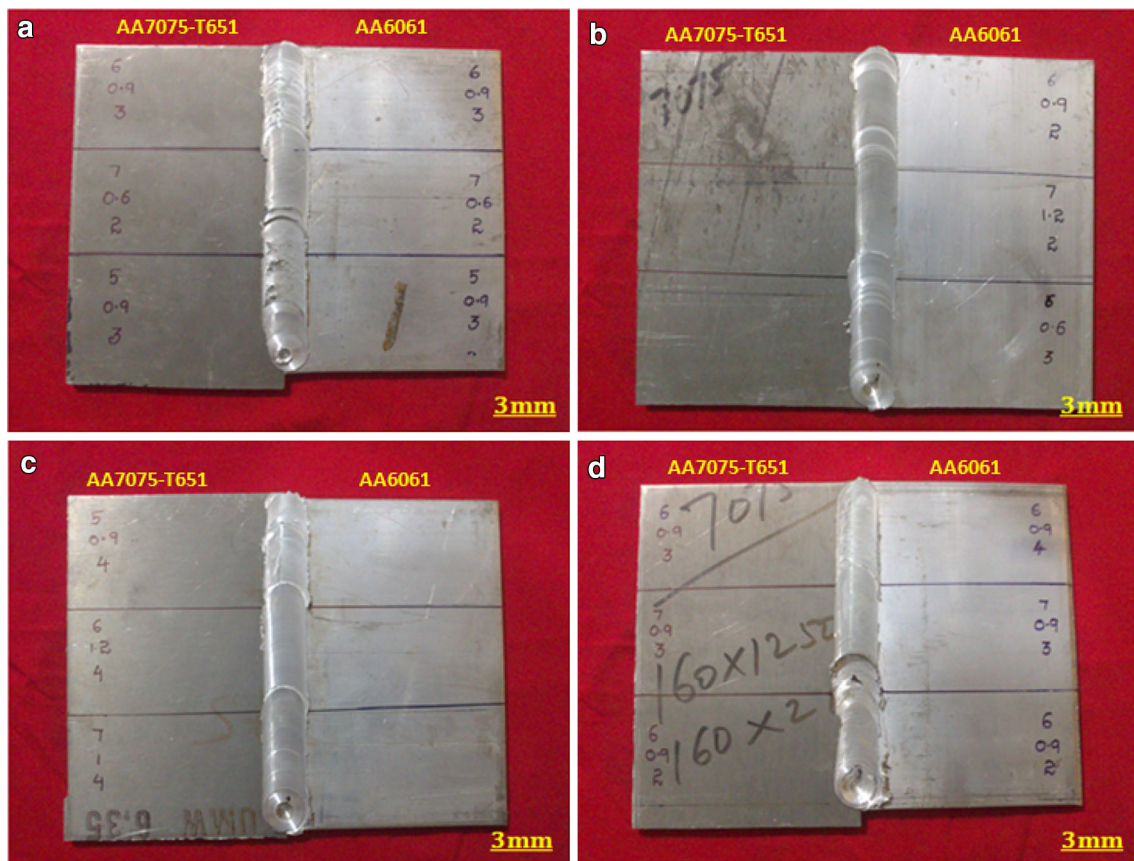
Fig. 4 Photograph of friction stir welded plates

FSW joint. Moreover, the etched specimen could be examined for grain size and its morphology. The Clemex image analysis software [31] was used to measure the average size of the grain by analysing a minimum of three images per sample. The image analysis software differentiates the dissimilar grains by exhibiting various grain morphologies. Finally, the software calculates the corresponding equivalent diameter D_{EQ} of each grain. The chemical compositions like Cu, Al, Mg, Zn and Si available in the weld region and tensile fractured surface were evaluated by using SEM–EDAX area scanning and line scanning techniques [32]. Metallographically specimens were prepared and etched before SEM–EDAX analysis. Then, the specimens were covered with cotton cloth to avoid surface damage and oxidation. The precipitated phase in the friction stir welded dissimilar joint was evaluated by using X-Ray Diffraction (XRD) analysis [33].

3 Results and Discussion

The results and discussion section includes (a) surface appearance and macrostructure, (b) material flow and microstructure analysis, (c) interface region analysis and

grain size measurement, (d) investigation of tensile behaviour, (e) investigation of microhardness, (f) analysis of bending strength and (g) tensile fracture surface morphology.

3.1 Surface Appearance and Macrostructure

The tool shoulder concave angle controls the contact between the shoulder bottom and workpiece surface. It regulates the temperature and plastic deformation of the material in the stir zone. When the tool shoulder concave angle increases, the volume of material flow also varies with the depth and volume of concave profile as shown in Table 3. The pulsating stirring action of the square pin (130 pulses/s) and triangle pin (100 pulses/s) forces the plasticized material to flow quickly inside the volume of tool shoulder concave angle. Therefore, there is no sticking of material in the tool shoulder with 4.5° concave angle. On the other hand, the tool pin profile determines the amount of material to be sheared and mixed in the stir zone [34]. These two factors decide the surface morphology and material flow in the weld region. The surface morphology and macrograph of all the weld joints exhibit defect-free region [35] except joints 1 and 7 as shown in Table 4. In
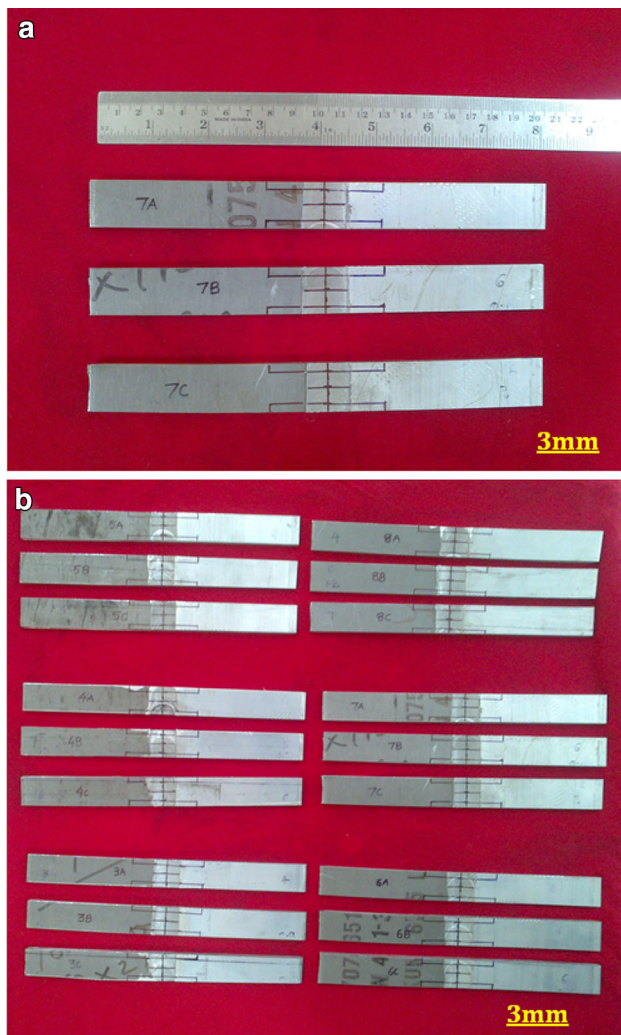
Fig. 5 Scheme of extraction of tensile specimens from dissimilar welded plates

the joint 1, galling is caused by excessive heat generation due to low concave angle in tool shoulder of tool T1 which leads to more surface contact between shoulder and workpiece. In the galling, the plasticized material stick to the straight cylindrical tool pin of tool T1 and the weld zone displays rough surface in the weld with tunnel formation due to lack of fill [36] as shown in Fig. 7. Furthermore, the low concave angle exerts excessive tool plunge force which exhibits flash formation in the weld surface. The FSW tool T7 shears more amount of material in the weld stir zone (WSZ) due to more static to dynamic volume ratio[14, 37, 38]. Moreover, the tool shoulder with 1.5° concave angle has close contact with the weld surface. The plasticized material flow inside the reduced volume of 1.5° shoulder has no relief time to decline the temperature. This excess heat generation leads to sticking of material and tunnel formation in the joint 7, as shown in Fig. 8. The dissimilar AA7075-T651 and AA6061 alloy joints

fabricated with square pin tool eradicate the sticking of material even in high heat input condition due to intense stirring action with even face (square four faces). Consequently, the surface morphology of all the welds fabricated by using square pin tool with different shoulder concave angles reveals better surface and macrostructure when compared to other joints.

3.2 Material Flow and Microstructure Analysis

Concave shoulder profile acts as a reservoir for collecting material during the stirring action of the pin. In cylindrical pin, the fluctuation of force is uniform with respect to time because of less amount of material deformation. On the other hand, even faced pin (square) exhibits higher forces [6, 38, 39] than the odd faced pin (triangle) as shown in Fig. 9. The axial force tends to decline while increasing the shoulder concave angle, which affects the horizontal and vertical flow of material around the pin profile. The optical micrograph of dissimilar AA7075-T651 and AA6061 joint fabricated with different tool shoulder concave angles and tool pin has been analysed and presented in this section. It has been observed that the obtained microstructures are entirely different from the microstructure which belongs to the joints fabricated with conventional FSW tool with flat end shoulder and cylindrical pin [22]. All these changes occur due to the combined effect of the tool shoulder concave angle (1.5°, 3° and 4.5°) and tool pin profiles (straight cylindrical, square and triangle). The tool shoulder concave profile plays a significant role on the material flow by applying the downward axial load to the material present below the shoulder region. Moreover, the ratio between the static volume and dynamic volume of tool pin profile determines the flow of the material path. This ratio for the straight cylindrical pin is 1, for square pin tool 1.36 and for triangular pin 2.65. The joint 1 fabricated by tool T1 exhibits excessive heat due to more surface contact between the tool shoulder and workpiece. The lack of material transformation is observed due to the sticking of plasticized material [40] in the straight cylindrical tool pin, and it leads to tunnel formation in the weld joint as shown in Fig. 10a. Figure 10b describes the influence of tool T2 on material flow in the weld stir zone. Tool T2 delivers sufficient temperature due to adequate frictional contact between the tool shoulder and workpiece. Furthermore, the straight cylindrical pin in this tool enhances the uniform material flow without any sticking and tunnel defect due to constant fluctuation of force. Microvoids are observed in the joint 3 fabricated by tool T3 due to inadequate coalescence of transferred material in the stir zone as shown in Fig. 10c. The joints fabricated with square pin tool with various concave shoulder angles exhibit flawless joint with excellent mechanical properties. The tool T4 accomplishes

Fig. 6 Photograph of tensile specimens (before testing)

Table 3 Depth and volume of tool shoulder concave profile with different angles

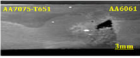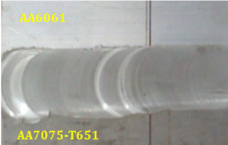| Sl. nos.	Tool used	Depth of concave (mm)	Volume of the concave (mm^3)
1.	Tool shoulder with 1.5° concave angle	0.261	27.41
2.	Tool shoulder with 3° concave angle	0.523	54.88
3.	Tool shoulder with 4.5° concave angle	0.785	82.41
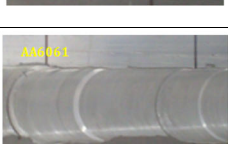
uniform material flow with fragment layer of metal transfer towards retreating side (AA6061) as shown in Fig. 10d. The tool T5 exhibits maximum hardness and tensile strength due to the combined effect of the square tool pin and concave shoulder. Moreover, this joint reveals the uniform flow of material along with onion ring formation [41] as shown in Fig. 10e. The tool T6 generates material flow stress in the stir zone (SZ) due to the temperature drop down of plasticized material inside the 4.5° shoulder concave angle. However, the sticking of material is avoided by pulsating stirring action of the square pin as shown in Fig. 10f. There is sliding friction between the plasticized material and concave profile shoulder with 1.5° angle in tool T7. Furthermore, excess heat input with intense stirring action [42] causes turbulent flow of material in the stir

zone and it leads to tunnel formation as shown in Fig. 10g. The FSW joint fabricated by tool T8 exhibits improved tensile strength and hardness triggered by uniform material flow with adequate shearing of plasticized material as shown in Fig. 10h. There is a localized strain due to thermal softening of material located in the outer edge of the tool T9 shoulder with 4.5° concave angle. The microstructure weakening can be retarded by varying the tool shoulder concave angle from 1.5° to 3°. The tool shoulder concave angle dominates the material flow and mechanical behaviour of the dissimilar aluminium alloy joint when compared to tool pin profile. Moreover, the intense stirring of odd faced tool pin (triangle) reveals moderate material flow without any defects in the weld joint 9 as shown in Fig. 10i.

3.3 Interface Region Analysis and Grain Size Measurement

The line scanning mode of EDAX technique has been employed to analyse the existence of various elements [43] in the weld stir zone (SZ). The concentration of aluminium in the stir zone of the dissimilar joint is more than other elements like magnesium (Mg), zinc (Zn), copper (Cu) and silicon (Si). The intensity of strengthening precipitate regulates the mechanical properties of the FSW joint. The weld centre of the joint 5 with good mechanical behaviour

Table 4 Surface morphology and macrograph of dissimilar joints fabricated with different tool geometries (shoulder and pin profile)

| Joint No.	Condition	Surface Appearance	Macrostructure	Quality of weld
1.	Tool with concave shoulder angle 1.5^0 and Straight cylindrical pin.(T1)			Tunnel formation
2.	Tool with concave shoulder angle 3^0 and Straight cylindrical pin.(T2)			Good
3.	Tool with concave shoulder angle 4.5^0 and Straight cylindrical pin.(T3)			Good
4.	Tool with concave shoulder angle 1.5^0 and Square pin.(T4)			Good
5.	Tool with concave shoulder angle 3^0 and Square pin.(T5)			Good
6.	Tool with concave shoulder angle 4.5^0 and Square pin. (T6)			Good
7.	Tool with concave shoulder angle 1.5^0 and Triangle pin.(T7)			Tunnel formation
8.	Tool with concave shoulder angle 3^0 and Triangle pin.(T8)			Good
9.	Tool with concave shoulder angle 4.5^0 and Triangle pin.(T9)			Good
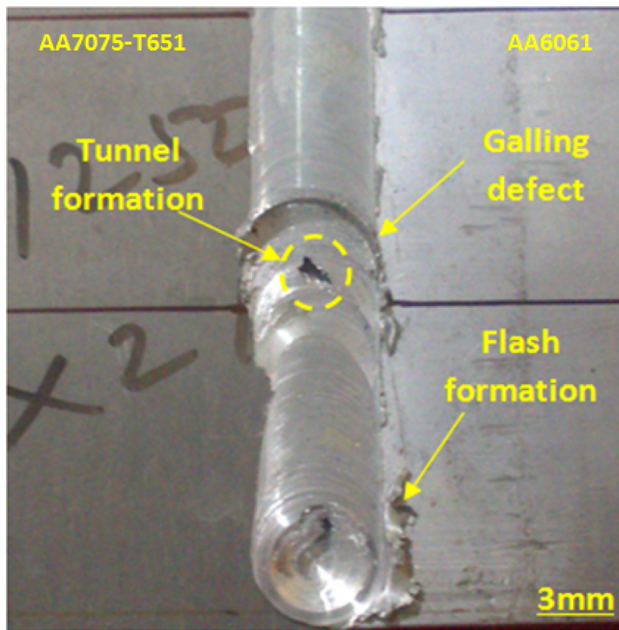
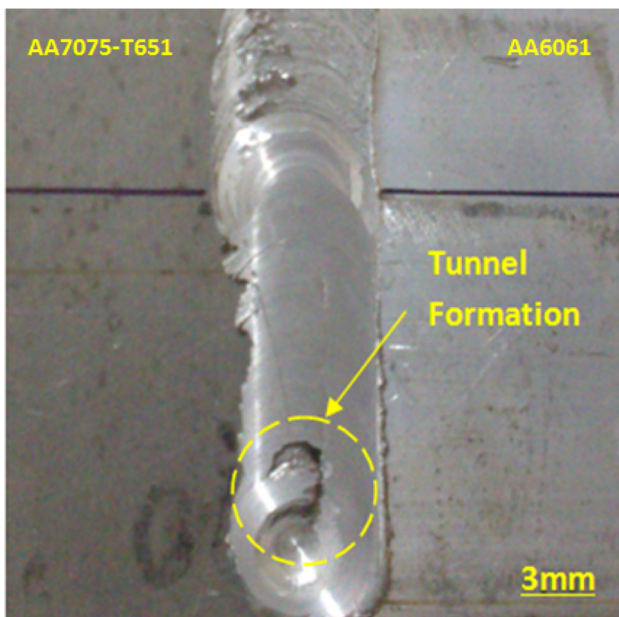**Fig. 7** Defects in the dissimilar joint 1 fabricated with FSW tool T1

Fig. 8 Defects in the dissimilar joint 7 fabricated with FSW tool T7

has been considered for line scanning technique. Figure 11a shows that the stir zone of the joint 5 exhibits a uniform, thin and continuous flow of IMCs material. The presence of strengthening precipitate $MgZn_2$ in the joint 5 is evident from the line scanning mode of EDAX technique and XRD as shown in Figs. 11b, c and 12. The pulsating stirring action of the square tool pin along with 3° concave shoulder provides sufficient flow of IMCs material and strengthening precipitates in the stir zone of joint 5. The tool shoulder concave angle exhibits the thermomechanical
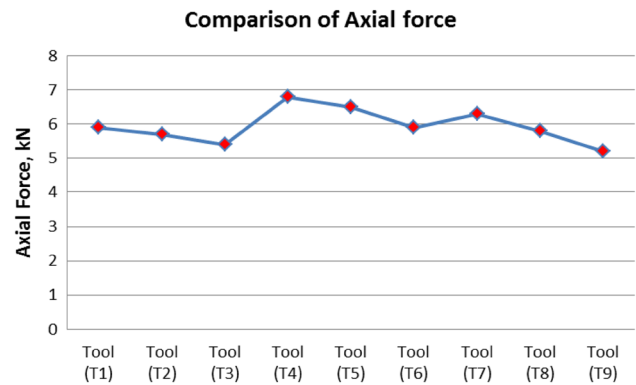

Fig. 9 Comparison of axial force

effect on the weld joint due to the forging action on the square pin sheared material. Moreover, this tool shoulder concave angle variation weakens the interaction between shoulder concave surface and the upward flow of square pin sheared material. This leads to the transfer of frictional heat for longer distance of the weld, which causes uniform flow of IMC without damage.

The grain size refinement during the FSW process determines the mechanical behaviour of the dissimilar joint. The concave shoulder improves the contact stability by keeping the plasticized material always in contact with the end surface of the tool. When compared to the straight cylindrical tool pin, square and triangular pin exhibits fine grains in the stir zone (SZ) due to the pulsating stirring action. On the other hand, the tool shoulder with the concave angle of 3° reveals fine grains due to dynamic recrystallization when compared to other tool shoulder angles. The joint 5 fabricated through tool T5 exhibits maximum tensile strength and hardness due to the combined effect of square pin tool and 3° shoulder concave angle. By and large, the grains located in the HAZ region become coarser due to localized deformation. Hence, the average grain size value of the HAZ region falls in between the values of WNZ and TMAZ region as shown in Fig. 13. Moreover, the straight cylindrical pin tools (T2, T3) reveal moderate mechanical properties due to coarse-grained formation when compared to square and triangular pin tools as shown in Fig. 14a. Figure 14b shows the sample of fine equiaxed grains [44] developed by square pin tools (T4, T5, T6) along with different concave shoulders. The triangular pin tools (T8, T9) demonstrate elongated grains with negligible grain boundary dislocations as shown in Fig. 14c.

3.4 Investigation of Microhardness

The influence of tool shoulder concave angle and pin profile on hardness profile across the dissimilar AA7075-

Fig. 10 Microstructure of
a joint 1, **b** joint 2, **c** joint 3,
d joint 4, **e** joint 5, **f** joint 6,
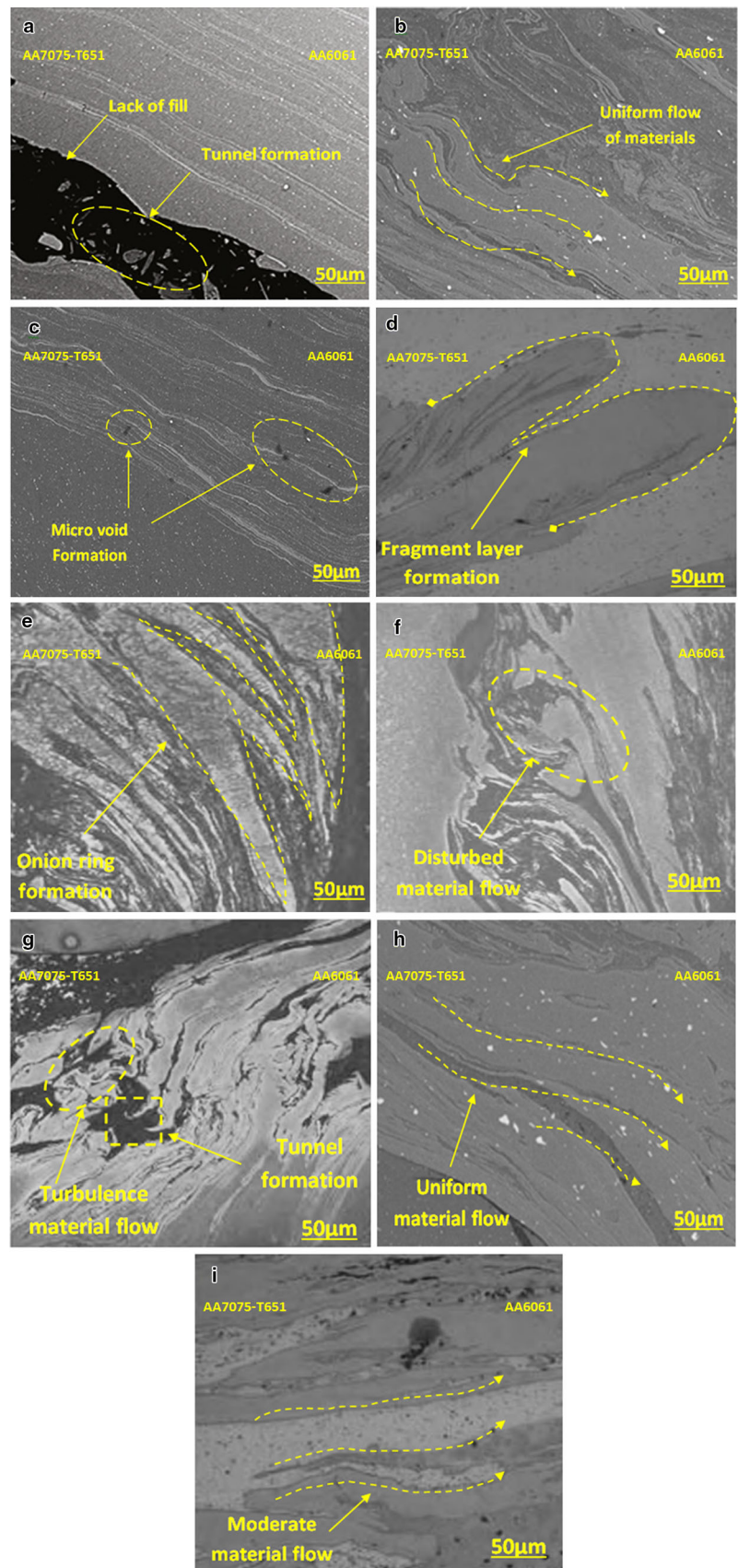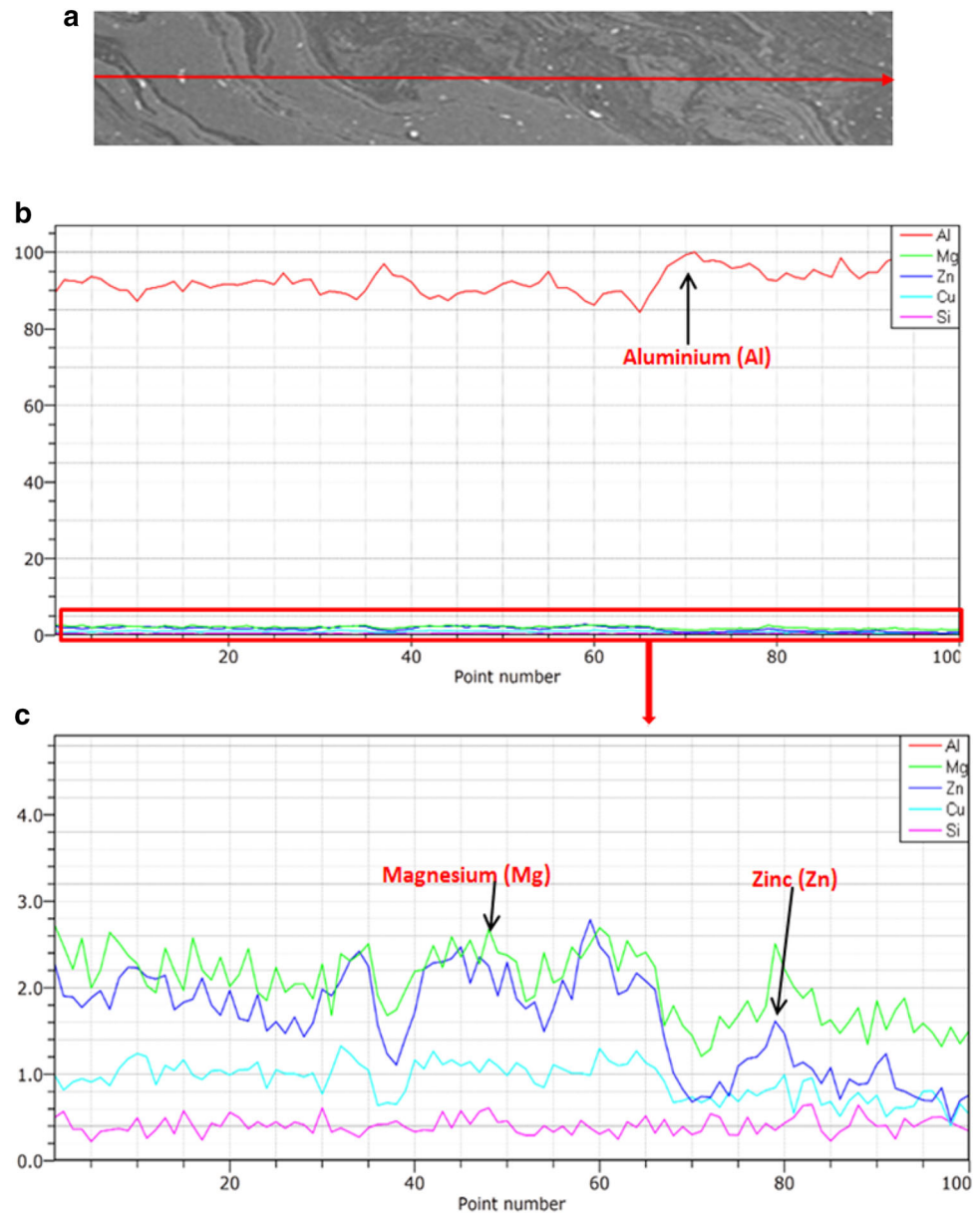**g** joint 7, **h** joint 8 and **i** joint 9

Fig. 11 Elements distribution analysis by using EDAX line scan of the FSW joint 5

T651 and AA6061 joint is shown in Fig. 15. The weak regions of the weld joint have been identified by measuring the hardness across five different zones such as i) weld stir zone (WSZ), ii) retreating side heat-affected zone (RSHAZ), iii) retreating side thermomechanically affected zone (RSTMAZ), iv) advancing side heat-affected zone (ASHAZ) and v) advancing side thermomechanically affected zone (ASHAZ). The dynamic recrystallization of grains, strengthening precipitates distribution and IMC material morphology determine the hardness profile across the weld joint. The joints 1 and 7 exhibit a minimum hardness value of 101 Hv and 103 Hv in the stir zone when compared to other joints fabricated with the different combinations of shoulder angle and pin profile. As mentioned in Sects. 3.1 and 3.2, excessive heat generation in

these two joints enlarges the grain size [45] and reduces the hardness value as shown in Fig. 16. This high heat input exhibits coarsening and dissolution of strengthening precipitates $MgZn_2$ in the joints 1 and 7. Moreover, the lack of material transformation and turbulence flow damages the thickness of the IMC layer in the stir zone of the joints 1 and 7, respectively. The figure reveals that most of the weld joint hardness values decline in between the stir zone (WSZ) and heat-affected zone (HAZ) of retreating side and advancing side due to the dissolution of the strengthening precipitates [46]. Increasing the shoulder concave angle from 1.5° to 3° narrows the softening region of WSZ and improves the hardness. In the TMAZ region, grain growth occurs without dynamic recrystallization. These are the root cause for few tensile specimens to get fractured in
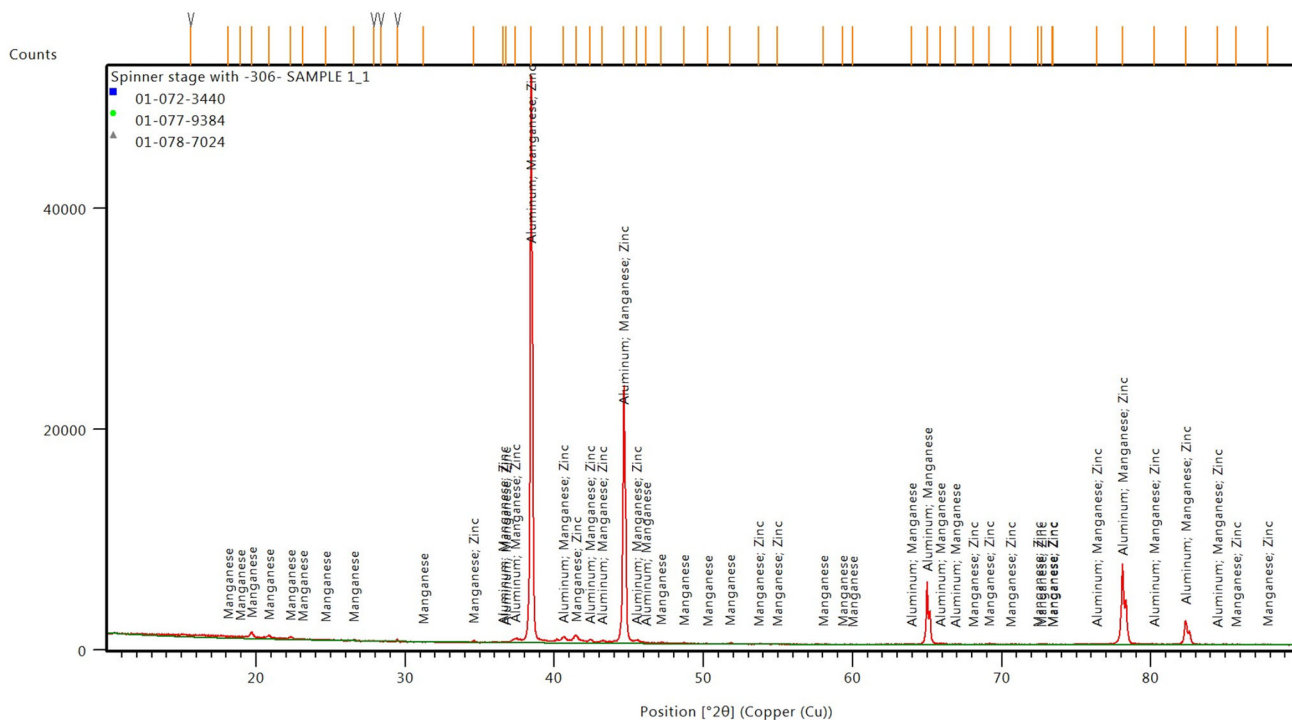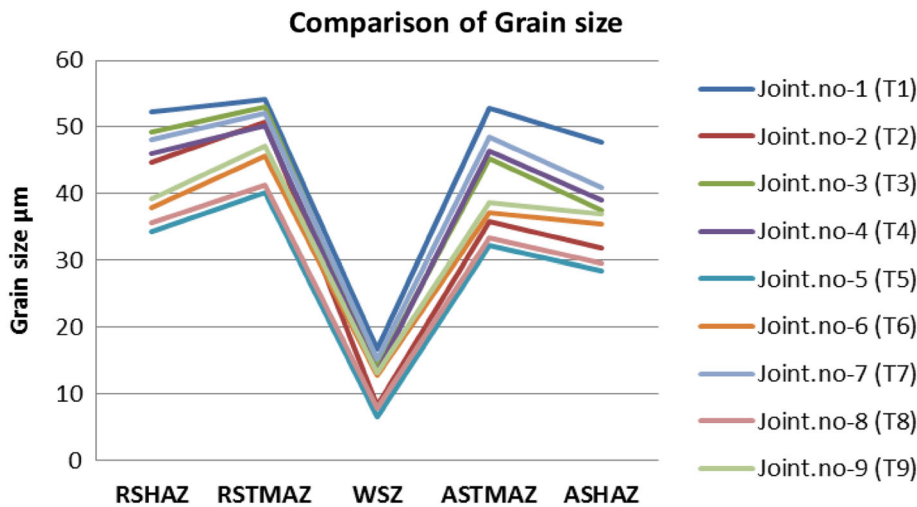
Fig. 12 XRD analysis of the FSW joint 5

Fig. 13 Grain size measurement comparison

between the WSZ and HAZ of the dissimilar joint. The joints 4, 5 and 6 fabricated by square pin tool with the different shoulder concave angles (T4, T5 and T6) exhibit uniform material flow due to pulsating stirring action. Furthermore, the joint 5 exhibits uniform and continuous flow of IMC layer with adequate thickness exhibiting a maximum hardness of 143 Hv.

3.5 Investigation of Tensile behaviour

The measured tensile properties of the dissimilar AA7075-T651 and AA6061 joint such as (1) yield strength, (2)

tensile strength, (3) % elongation and (4) joint efficiency are shown in Figs. 17, 18, 19 and 20. The joint efficiency is calculated by using the formula:

$$\% \text{ Joint efficiency} = \frac{\text{Tensile strength of the weld joint} \times 100}{\text{Tensile strength of AA6061}}$$

The ratio of static to the dynamic volume determines the material flow in the stir zone. The square pin (1.36) and triangular pin (2.65) dominate the material shear and flow behaviour in the stir zone when compared to the straight pin tools. On the other hand, the variation in heat generation and the axial force due to different tool

Fig. 14 Microscopic view of **a** coarsened grains in joint 2, **b** equiaxed fine grains in joint 5 and **c** elongated grain boundary dislocation in joint 8
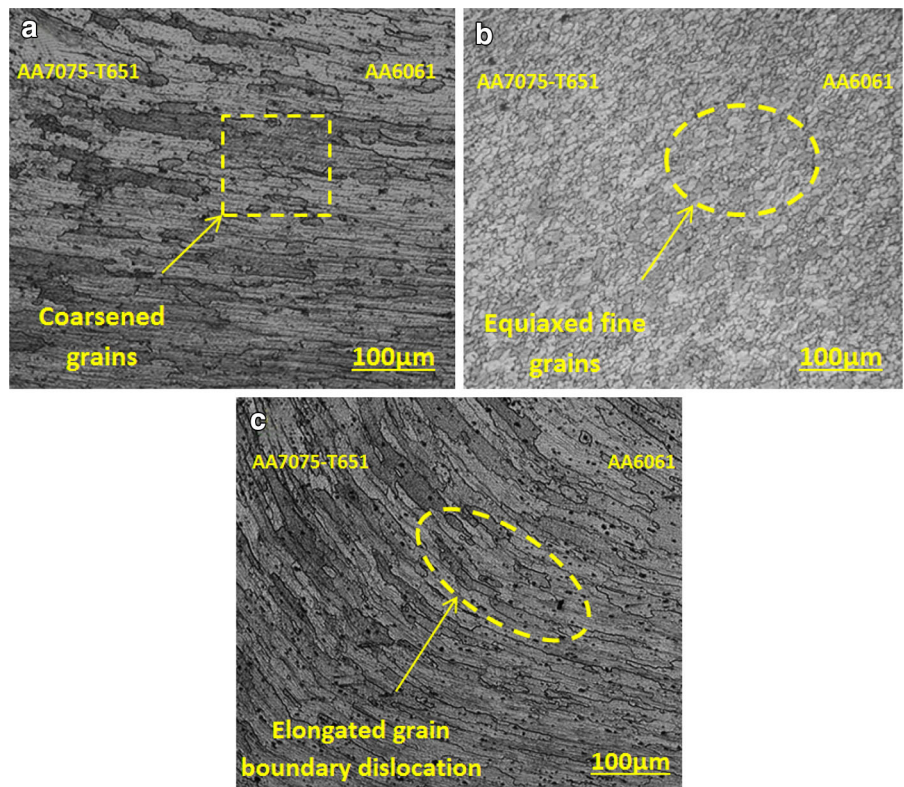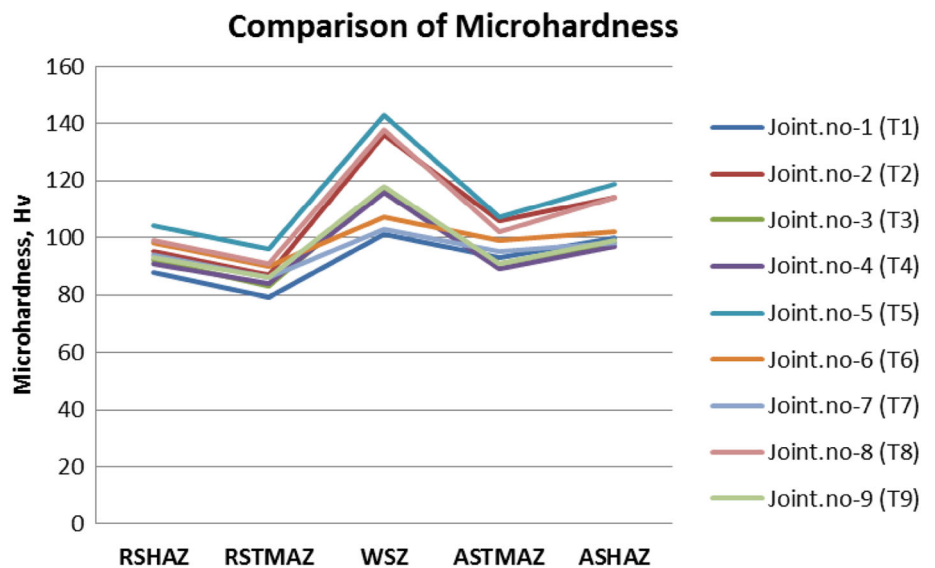

Fig. 15 Comparison of weld joint microhardness

shoulder concave angles affects the material flow support from the tool pin and declines the mechanical behaviour of the friction stir welded dissimilar joint. In the joints 1 and 7, the tensile fracture initiates from the centre of the weld stir zone (SZ) and propagates along the TMAZ region as shown in Fig. 21. The tensile strength of the joints 1 and 7 decline while increasing the shoulder concave angle to 4.5°. The lack of material transformation and increased grain size in between the stir zone (SZ) and HAZ due to

excess heat generation declines the tensile strength of the joint 1–232 Mpa with 74.8% joint efficiency. Furthermore, the joint 1 fabricated through tool T1 reveals minimum tensile strength and hardness due to a non-homogeneous flow of IMCs material and tunnel formation in the stir zone of the dissimilar joint. In joint 7, the triangular pin generates turbulence flow of material with excessive heat, which increases the grain size and weakens the tensile strength [47] of the joint 7–239 Mpa with 77.1% joint

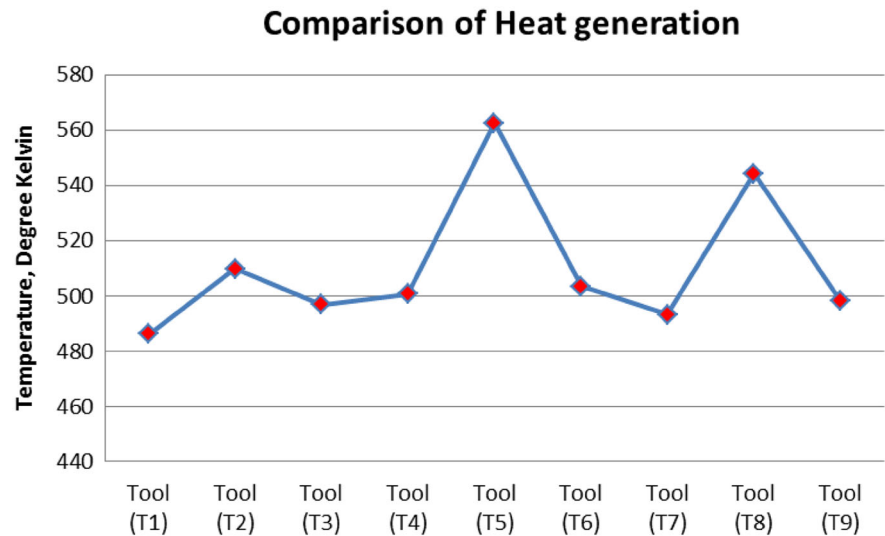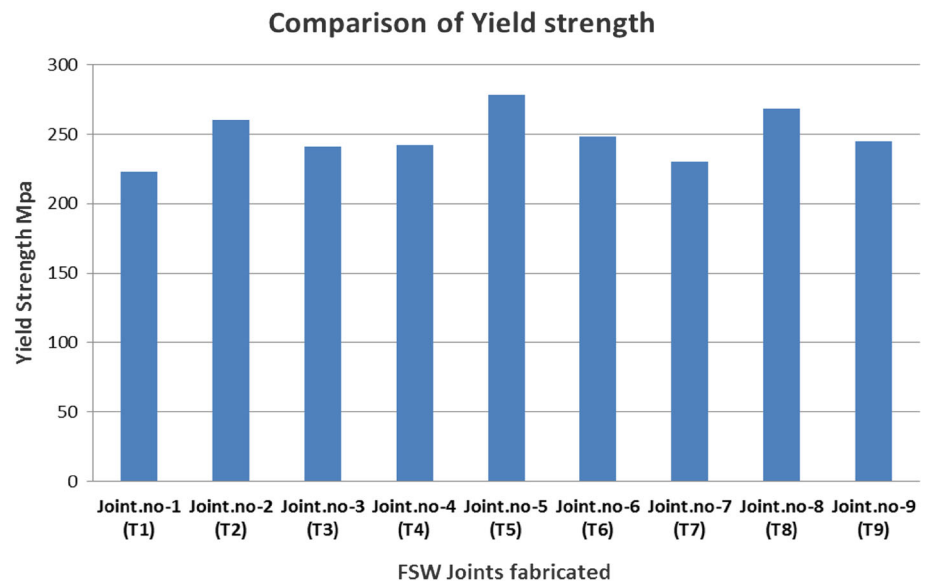**Fig. 16** Comparison of heat generation in different FSW tools

**Fig. 17** Comparison of weld joint yield strength

efficiency. The square pin and triangular pin tool with 3° shoulder concave angle exhibit maximum tensile strength of 298 and 289 Mpa, respectively, when compared to other tools. In addition, the triangular and square pin profiles produce a pulsating stirring action in the flowing material due to flat faces. The square pin and triangular pin generate the pulse of 130 pulses/s and 100 pulses/s, respectively, at the tool rotational speed of 2000 rpm. There is no such pulsating action in the case of triangle and cylindrical pin profiles. This pulsating stirring action improves the joint efficiency of joints 5 and 8 to 96.1% and 93.2%, respectively, due to uniform material flow, IMC material morphology and distribution of fine strengthening precipitates [48]. The hardness distribution reveals that the region between the weld stir zone (WSZ) and heat-affected zone (HAZ) is weak [49]. This causes most of the

tensile specimens to get fractured in between the WSZ and HAZ [50] as shown in Fig. 22.

3.6 Tensile Fracture Surface Morphology

Fractography has been used to study the tensile fractured surface of the dissimilar weld joint and to analyse the causes for joint failure (ductile or brittle). The field emission scanning electron microscope (FESEM) has been employed to study the failure patterns in the tensile fractured surface. The FSWed joint 1 fabricated by using the straight cylindrical pin with 1.5° shoulder concave angle exhibits minimum tensile strength and hardness. The formation of large voids and cleavage type [51] fracture mode is observed due to the poor ductility of the weld joint as shown in Fig. 23a. The ductile property of these joints

Fig. 18 Comparison of weld joint tensile strength
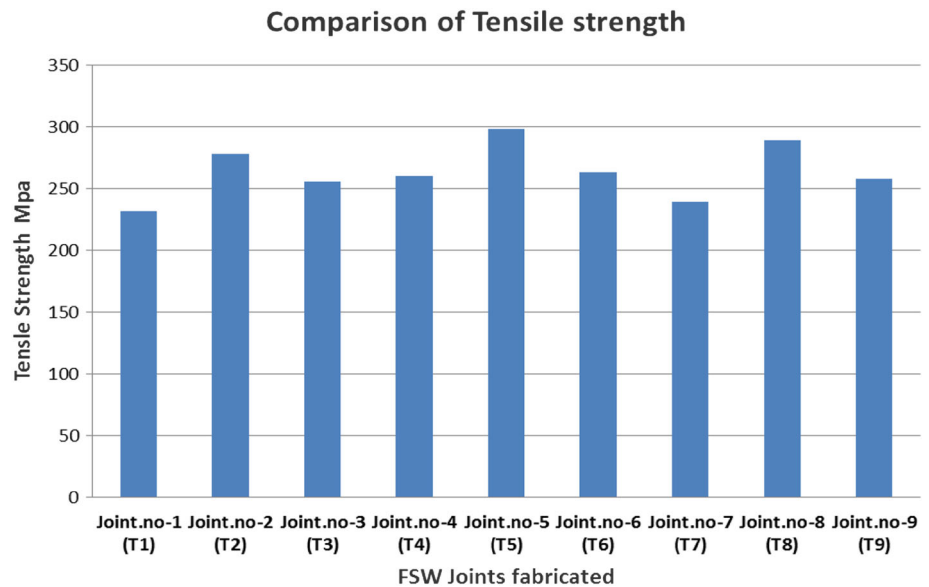
Fig. 19 Comparison of elongation percentage
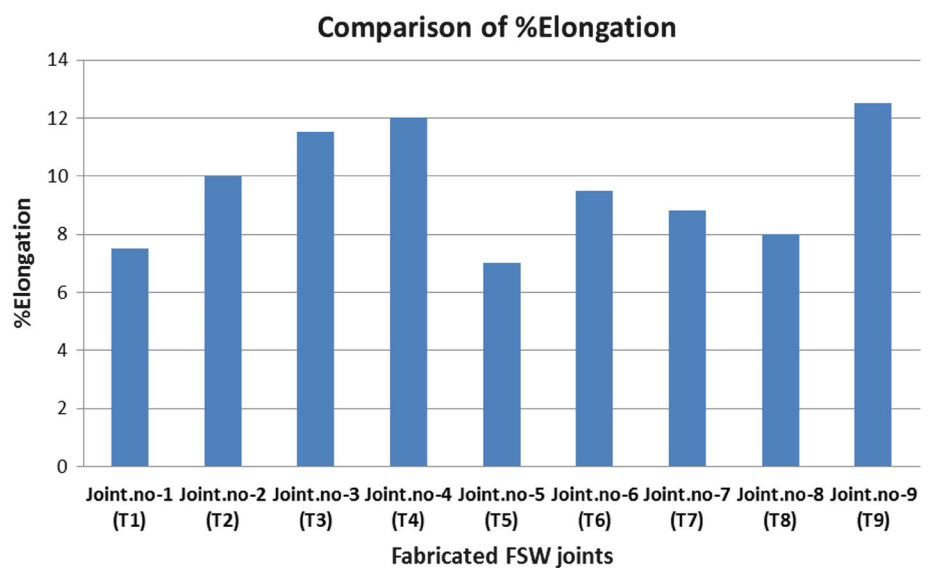
decline due to lack of material transformation (material filling in the stir zone), tunnel formation and lack of strengthening precipitate distribution. The straight cylindrical tool pin exhibits fine dimples with tear ridges along the weld stir zone as shown in Fig. 23b. Furthermore, few elongated dimples are also observed along the boundary between the WSZ and TMAZ of joint 2 due to the fluctuation of force exhibited by straight cylindrical pin. On the other hand, a mixture of elongated and sheared dimples is witnessed in a zig–zag pattern in the joint 3 due to lack of axial force and poor coalescence of transferred material as shown in Fig. 23c. The combination of cleavage and dimples in the FSWed joint 4 reveals the mixed mode of brittle and ductile fracture in the stir zone (WSZ) as shown in Fig. 23d. The fragmented layer of material flow in the

stir zone is the primary cause for the mixed mode of fracture. The pulsating stirring action of the square pin tool with 3° shoulder concave angle demonstrates very fine dimples [52] in the joint 5 as shown in Fig. 23e. This ductile mode of fracture matches well with the measured tensile properties such as yield strength, ultimate tensile strength and %elongation. The material flow stress in the joint 6 due to the temperature drop down of the plasticized material in the stir zone exhibits dimples with shear and shrinkage as shown in Fig. 23f. The fractured surface of the joint 7 with minimum tensile strength exhibits microvoids [53], and cleavage planes are shown in Fig. 23g. This brittle mode of fracture happens due to the turbulence of material and inadequate distribution of strengthening precipitates in the WSZ. The intense stirring of the triangular
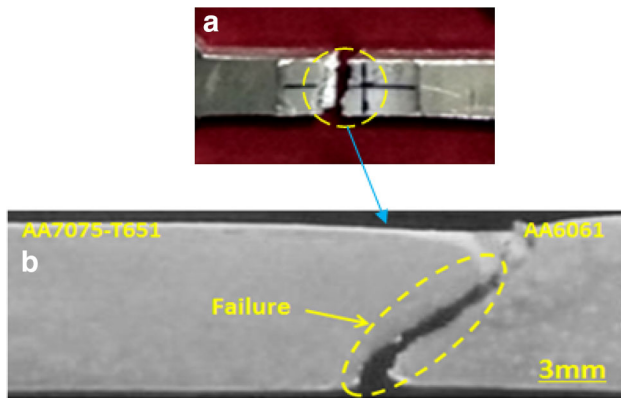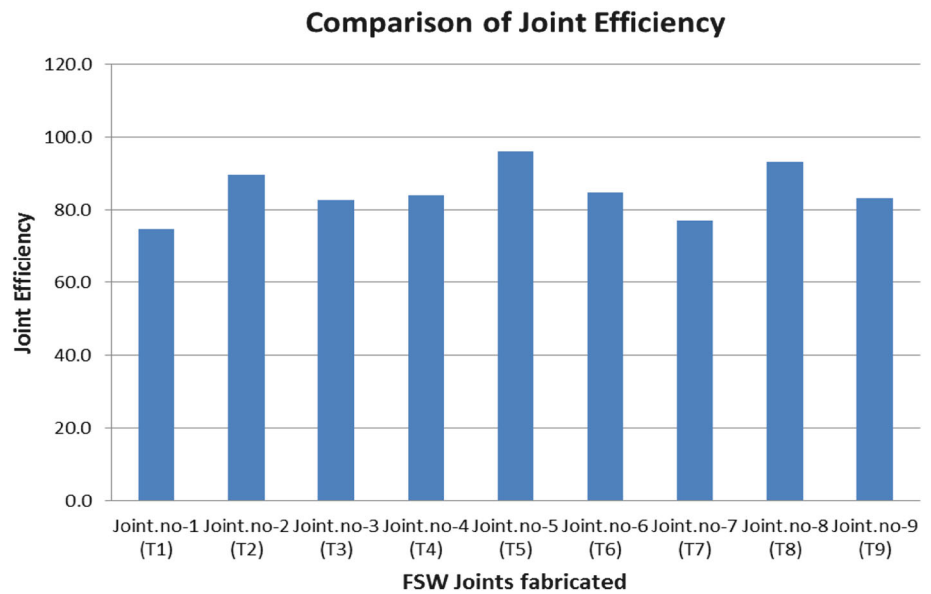
Comparison of Joint Efficiency

Fig. 21 Macroscopic view of tensile failure joint

pin along with 3° shoulder concave angle exhibits excellent mechanical properties in the joint 8 due to uniform distribution of fine dimples along the WSZ of the fractured surface as shown in Fig. 23h. The FSWed joint 9 exhibits sheared and elongated dimples [54] along the stir zone due to the localized strain of material located at the outer edge of the concave profile shoulder as shown in Fig. 23i. The joints 5 and 8 exhibit better mechanical behaviour due to the uniform distribution of strengthening precipitates $MgZn_2$, which is evident from the EDAX analysis as shown in Fig. 24a, b.

3.7 Investigation of Bending Strength

The bending angle (BA) determines the resistance of the FSWed dissimilar AA7075-T651 and AA6061 joint against the compressive load [55]. The ductility and soundness of the weld joint have been evaluated by using the bending test. Moreover, this test has been conducted to ensure the
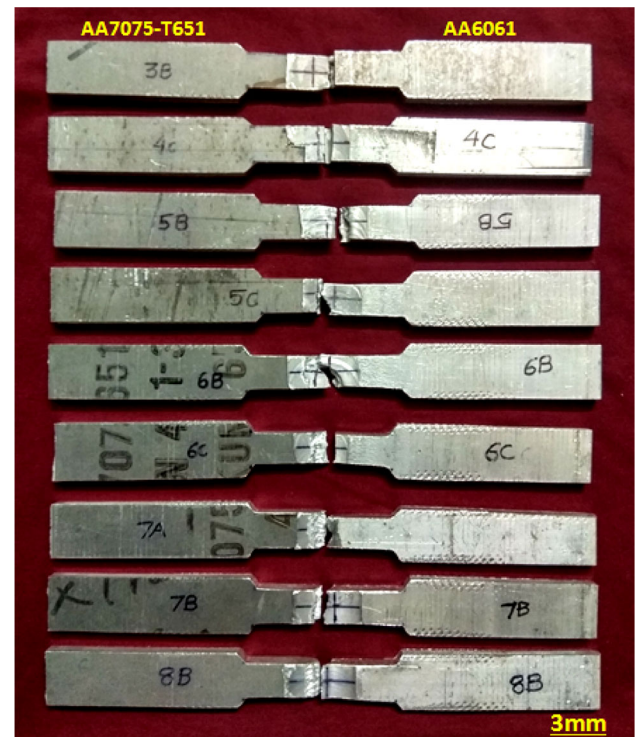

Fig. 22 Photograph of tensile specimens (after testing)

fusion between the weld and parent material. The bending test has been carried out by employing two different methods such as (a) face bend test and (b) root bend test. As mentioned in Sect. 2.3.3, three-point roller bending test set-up in the uniaxial fatigue testing machine has been used for the test as shown in Fig. 25a, b. The tunnel formation leads to the fracture of joints 1 and 7 at the weld stir zone (WSZ) in both face and root tests when a compressive load is applied. Lack of material transformation and excessive

Fig. 23 SEM images of tensile fracture surface of : **a** joint 1, **b** joint 2, **c** joint 3, **d** joint 4, **e** joint 5, **f** joint 6, **g** joint 7, **h** joint 8 and **i** joint 9
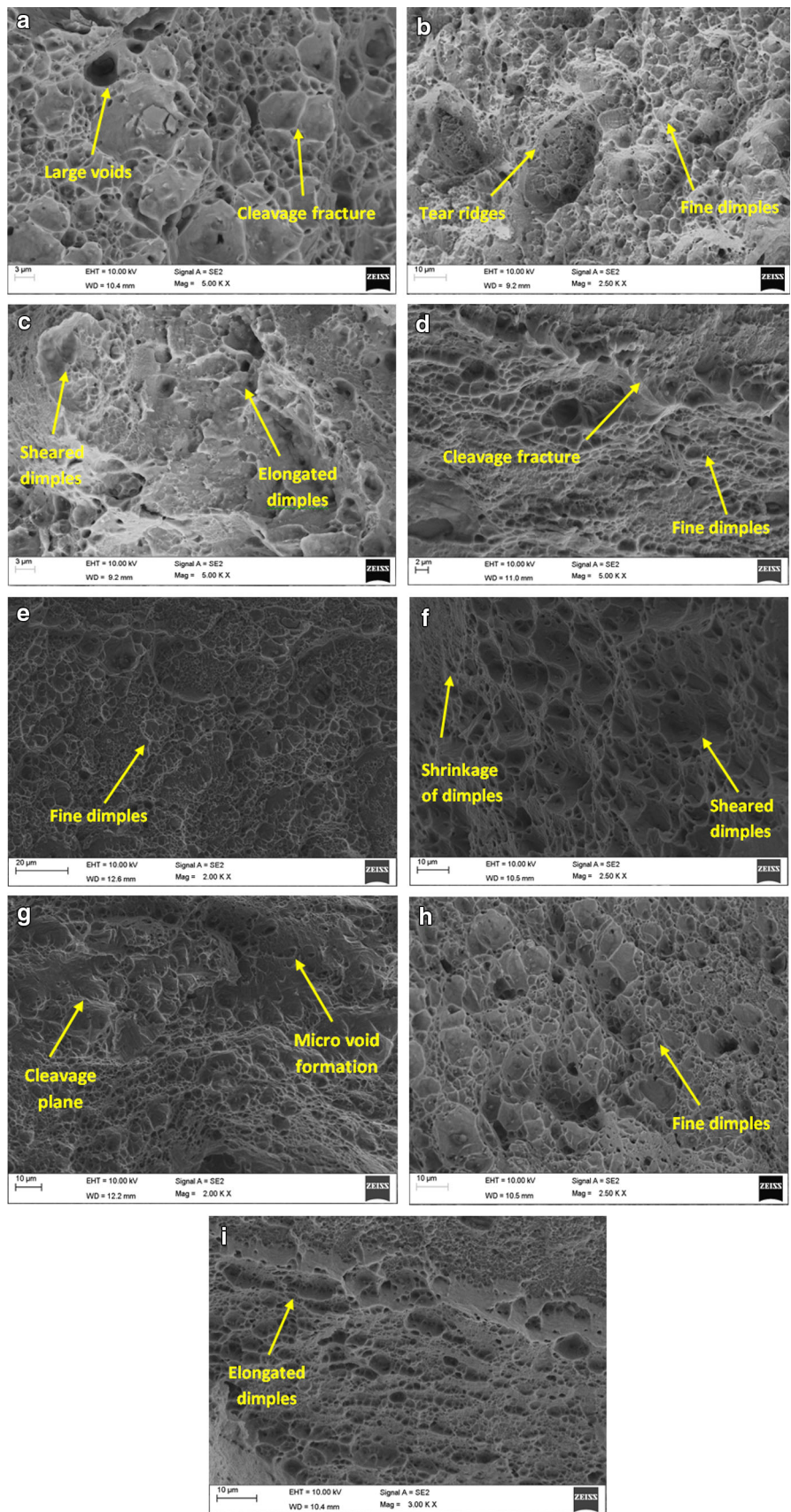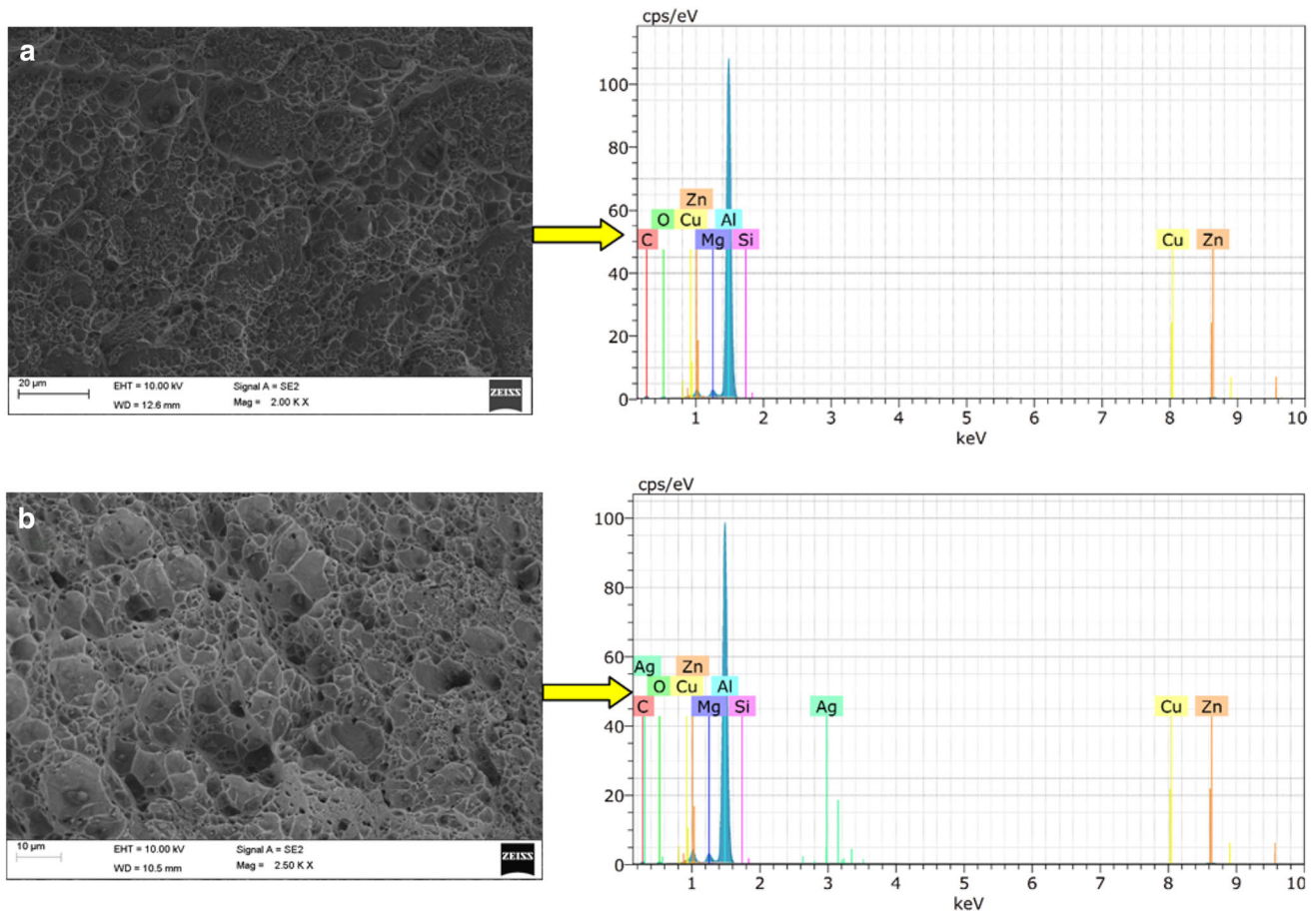
Fig. 24 EDAX analysis of the tensile fracture surface of: **a** joint 5 and **b** joint 8
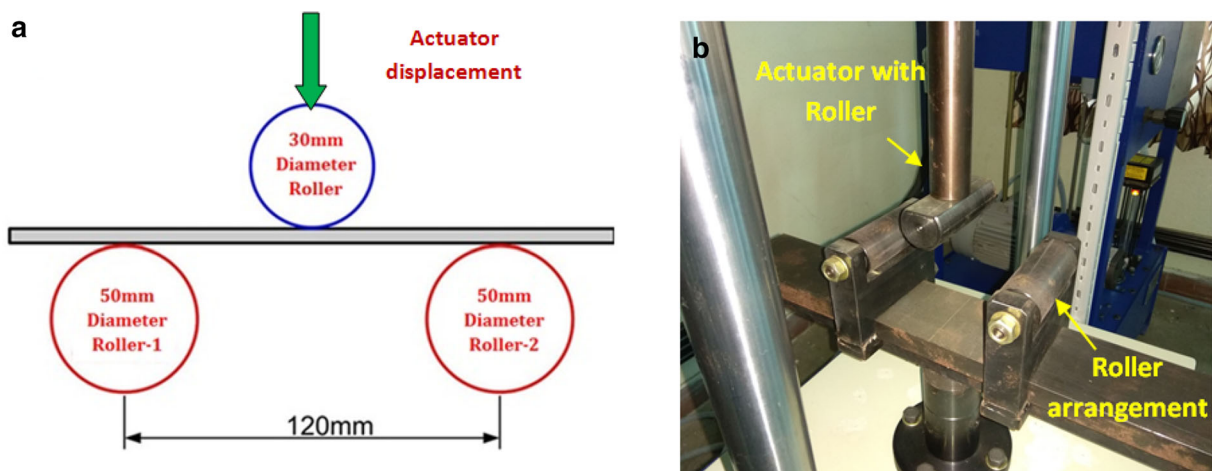

Fig. 25 **a** Schematic illustration of three-point bend test set-up and **b** photograph of bend test set-up

turbulence in the stir zone deteriorates the bonding strength of the joint to resist the bending. The crack initiates from the tunnel region and propagates towards the face and root [56] during the respective bend test. The joints 5 and 8 exhibit the maximum bending angle when compared to other joints as shown in Fig. 26. The maximum bending angle (BA) value indicates the better resistance of the dissimilar joint against the compressive load. Moreover, there is no evidence of crack formation and failure is observed in these joints. Joint 5 reveals the maximum

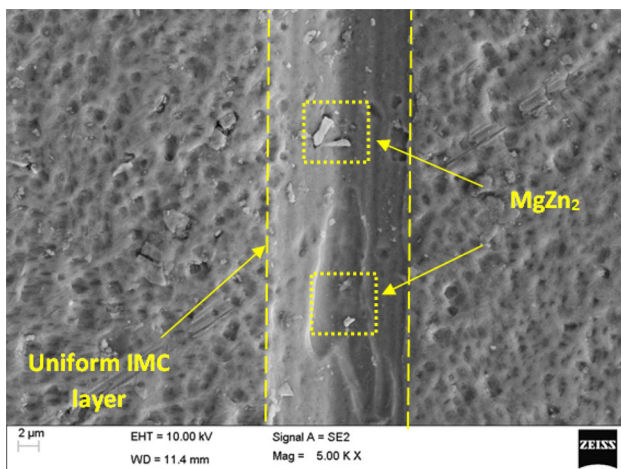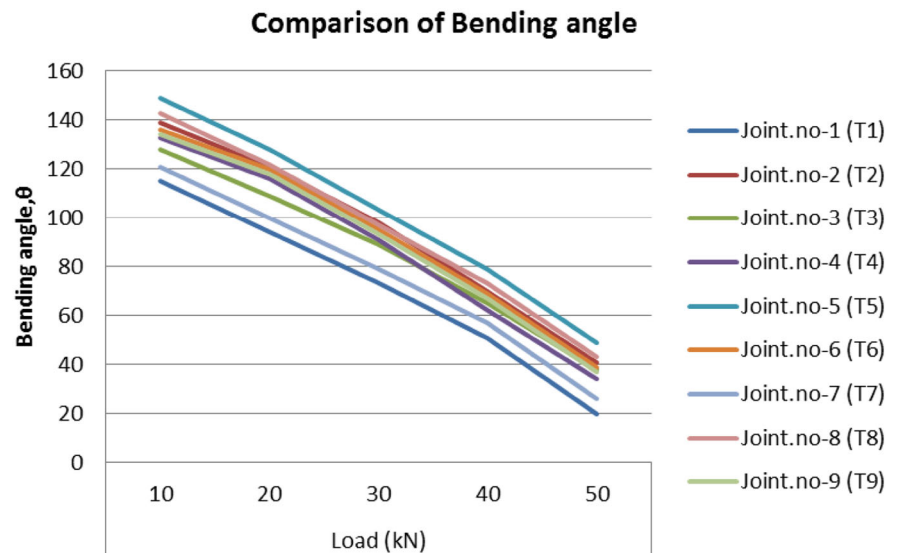Fig. 26 Comparison of bending angle with load variation

Fig. 27 SEM image of uniform IMC layer in the joint 5

bending angle of 49° due to the formation of uniform IMC layer in the stir zone which improves the bonding strength as shown in Fig. 27. Furthermore, the pulsating stirring action of the square tool pin exhibits uniform material flow through concave shoulder with strengthening precipitate $MgZn_2$ in the weld stir zone, and it is evident from the XRD analysis shown in Fig. 28. U-bend test has also been conducted in the dissimilar joint to evaluate the soundness of weld and to display the sub-surface defects like voids and tunnel formation. Similar to three-point test, joints 5 and 8 resist well against the compressive load and also replicate the shape of U-bend die without any defects as shown in Fig. 29a. Nevertheless, the joints 1 and 7 fail to withstand the load and get fractured due to lack of bonding and tunnel formation as shown in Fig. 29b.

4 Conclusion

In this present study, the influence of tool shoulder concave angle and tool pin profile on mechanical properties and microstructural behaviour of AA7075-T651 and AA6061 dissimilar joint has been investigated. This experimental investigation has been conducted by using three different shoulder concave angles (1.5°, 3° and 4.5°) and three different pin profiles (straight cylindrical, square and triangle). Based on the experimental work and results obtained, the following results are obtained:

1. The tool shoulder concave angle of 3° and square tool pin combination exhibits better surface morphology, mechanical properties (tensile properties, microhardness and bending strength) and microstructural behaviour of the joint.

2. The ratio between the static volume and the dynamic volume of square tool pin (1.36) combines with 3° tool shoulder concave angle (tool T5—joint 5), which exhibits better surface morphology and uniform material flow in the stir zone.

3. The microstructural analysis of the joint 5 exhibits uniform and continuous flow of IMCs material and strengthening precipitates $MgZn_2$ in the stir zone (WSZ) to maximize the mechanical behaviour (tensile strength, microhardness and bending strength).

4. The microhardness measurement profile across the joint 5 reveals the maximum hardness of 143 Hv when compared to other joints. The combination of 3° tool shoulder concave angle and square pin tool exhibits a uniform layer of IMC with adequate thickness to resist the indenter to penetrate stir zone, which improves the hardness of the joint 5.
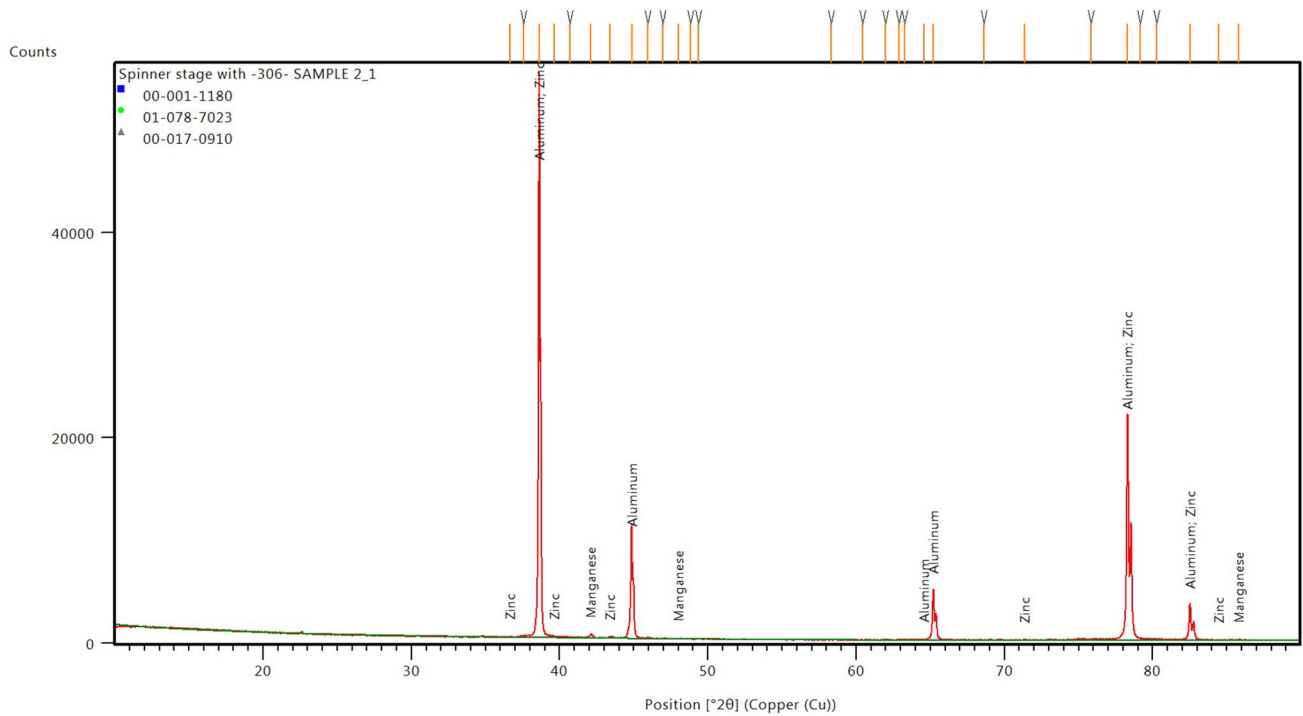
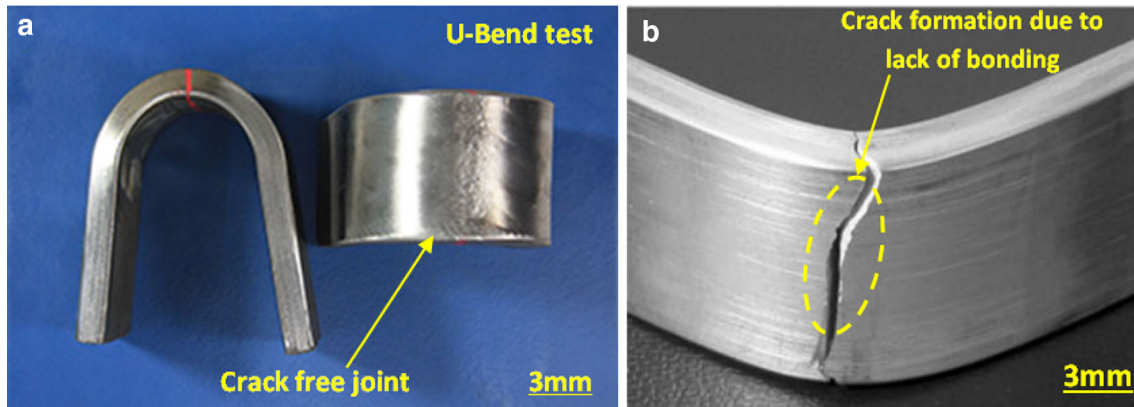**Fig. 28** XRD analysis of the bend specimen (joint 5)

Fig. 29 **a** Photograph of U-bend test specimen (joint 5) and **b** U-bend test specimen (joint 1)

5. The FSWed joint 5 fabricated by employing 3° tool shoulder concave angle, and square pin tool exhibits the maximum tensile strength of 298 Mpa with 96.1% joint efficiency. The ductility of this joint has been enhanced by uniform material flow and adequate distribution of strengthening precipitate ($MgZn_2$).

6. The formation of the IMC layer with an adequate distribution of strengthening precipitate ($MgZn_2$) in the joint 5 resists the maximum bending load of 5OkN and exhibits the maximum bending angle of 49° without any crack formation. Similarly, the joint 5 resists the bending in the U-bend test and replicates the U-shaped profile of the die without any damage.

7. The presence of fine dimples along the tensile fractured surface of the joint 5 exhibits the ductile mode of failure. Furthermore, the EDAX analysis of the fractured surface reveals the adequate presence of strengthening precipitate ($MgZn_2$) to maximize the mechanical behaviour (tensile strength, microhardness and bending strength) of the dissimilar joint.

References

1. Ragu Nathan S, Balasubramanian V, Malarvizhi S, and Rao A G, *Trans Indian Inst Met* **69** (2016) 1861.

2. Reza-E-Rabby M, Tang W, and Reynolds A P, *Sci Technol Weld Join* **20** (2015) 425.
3. Sharma C, Dwivedi D K, and Kumar P, *Mater Des* **43** (2013) 134.
4. Rambabu G, Balaji Naik D, Venkata Rao C H, Srinivasa Rao K, and Madhusudan Reddy G, *Def Technol* **11** (2015) 330.
5. Galvão I, Leal R M, Rodrigues D M, and Loureiro A, **213** (2013) 129.
6. Mugada K K, and Adepu K, *Alloy J Inst Eng Ser C* (2018).
7. Leal R M, Leitão C, Loureiro A, Rodrigues D M, and Vilaça P, *Mater Sci Eng A* **498** (2008) 384.
8. Mugada K K, and Adepu K, *J Manuf Process* **32** (2018) 625.
9. Scialpi A, De Filippis L A C, and Cavaliere P, *Mater Des* **28** (2007) 1124.
10. Trueba L, Heredia G, Rybicki D, and Johannes L B, *J Mater Process Technol* **219** (2015) 271.
11. Palanivel R, Koshy Mathews P, Murugan N, and Dinaharan I, *Mater Des* **40** (2012) 7.
12. Mehta K P, and Badheka V J, *Trans Nonferrous Met Soc China* **27** (2017) 36.
13. Beygi R, Mehrizi M Z, Verdera D, and Loureiro A, *J Mater Process Technol* **255** (2018) 739.
14. Elangovan K, and Balasubramanian V, (2007) 163.
15. Ilangovan M, Rajendra Boopathy S, and Balasubramanian V, *Def Technol* **11** (2015) 174.
16. Elangovan K, Balasubramanian V, and Valliappan M, *Mater Manuf Process* **23** (2008) 251.
17. Motalleb-nejad P, Saeid T, Heidarzadeh A, Darzi K, and Ashjari M, *Mater Des* **59** (2014) 221.
18. Bahrami M, Besharati Givi M K, Dehghani K, and Parvin N, *Mater Des* **53** (2014) 519.
19. Kim J-R, Ahn E-Y, Das H, Jeong Y-H, Hong S-T, Miles M, and Lee K-J, *Int J Precis Eng Manuf* **18** (2017) 445.
20. Zhang H J, Wang M, Zhu Z, Zhang X, Yu T, and Wu Z Q, (2018).
21. Sathiya P, Aravindan S, and Haq A N, *Int J Adv Manuf Technol* **26** (2005) 505.
22. Yuvaraj K P, Varthanan P A, and Rajendran C, **7** (2018) 130.
23. Aliha M R M, Shahheidari M, Bisadi M, Akbari M, and Hossain S, *Int J Adv Manuf Technol* **86** (2016) 2551.
24. Sahu P K, Pal S, Pal S K, and Jain R, *J Mater Process Technol* **235** (2016) 55.
25. Sevvel P, and Jaiganesh V, *Trans Indian Inst Met* **68** (2015) 41.
26. Hajihashemi M, Shamanian M, and Niroumand B, *Sci Technol Weld Join* **21** (2016) 493.
27. Safeen W, Hussain S, Wasim A, and Jahanzaib M, (2016).
28. Paventhan R, Lakshminarayanan P R, and Balasubramanian V, *Trans Nonferrous Met Soc China* **21** (2011) 1480.
29. Golezani A S, Barenji R V, Heidarzadeh A, and Pouraliakbar H, *Int J Adv Manuf Technol* **81** (2015) 1155.
30. Dorbane A, Mansoor B, Ayoub G, Shunmugasamy V C, and Imad A, *Mater Sci Eng A* **651** (2016) 720.
31. Khodaverdizadeh H, Heidarzadeh A, and Saeid T, *Mater Des* **45** (2013) 265.
32. Chang W S, Rajesh S R, Chun C K, and Kim H J, *J Mater Sci Technol* **27** (2011) 199.
33. Heirani F, Abbasi A, and Ardestani M, *J Manuf Process* **25** (2017) 77.
34. Kamal Babu K, Panneerselvam K, Sathiya P, Noorul Haq A, Sundarrajan S, Mastanaiah P, and Srinivasa Murthy C V, *Surf Rev Lett* **25** (2017) 1850071.
35. Das U, Toppo V, Sahoo T K, and Sahoo R, *Trans Indian Inst Met* **71** (2018) 823.
36. Peddavarapu S, Raghuraman S, Bharathi R J, Sunil G V S, and Manikanta D B N S, *Trans Indian Inst Met* **70** (2017) 703.
37. Elangovan K, and Balasubramanian V, *Mater Sci Eng A* **459** (2007) 7.
38. Elangovan K, Balasubramanian V, and Valliappan M, *Int J Adv Manuf Technol* **38** (2008) 285.
39. Gopalakrishnan S, and Murugan N, *Mater Des* **32** (2011) 462.
40. Shi H, Chen K, Liang Z, Dong F, Yu T, Dong X, Zhang L, and Shan A, *J Mater Sci Technol* **33** (2017) 359.
41. Mastanaiah P, Sharma A, and Reddy G M, *Trans Indian Inst Met* **69** (2016) 1397.
42. Shiraly M, Shamanian M, Toroghinejad M R, Jazani M A, and Sadreddini S, *Trans Indian Inst Met* **70** (2017) 2205.
43. Kunnathur Periyasamy Y, Perumal A V, and Rajasekaran D, *Trans Indian Inst Met* (2018).
44. Reddy G M, Mastanaiah P, Prasad K S, and Mohandas T, *Trans Indian Inst Met* **62** (2009) 49.
45. Emamikhah A, Abbasi A, Atefat A, and Givi M K B, *Int J Adv Manuf Technol* **71** (2014) 81.
46. Mallieswaran K, Padmanabhan R, and Balasubramanian V, *Adv Mater Process Technol* **4** (2018) 142.
47. Saremi M L, Mirsalehi S E, and Shamsipur A, *Trans Indian Inst Met* **70** (2017) 1869.
48. Jaiganesh V, and Sevvel P, *Trans Indian Inst Met* **68** (2015) 99.
49. Priya R, Sarma V S, and Rao K P, *Trans Indian Inst Met* **62** (2009) 11.
50. Heidarzadeh A, Barenji R V, Esmaily M, and Ilkhichi A R, *Trans Indian Inst Met* **68** (2015) 757.
51. Rasaee S, Mirzaei A H, Almasi D, and Hayati S, *Trans Indian Inst Met* **71** (2018) 1553.
52. Sivaraj P, Kanagarajan D, and Balasubramanian V, *Def Technol* **10** (2014) 1.
53. Mehta K P, and Badheka V J, *Mater Manuf Process* **31** (2016) 233.
54. Liu X C, Wu C S, and Padhy G K, **20** (2015) 345.
55. Khan N Z, Siddiquee A N, Khan Z A, and Mukhopadhyay A K, *J Alloys Compd* **695** (2017) 2902.
56. Fowler S, Toumpis A, and Galloway, *Int J Adv Manuf Technol* **84** (2016) 2659.